

# Dynamics of Droplets and Mass Transfer in a Rotating Packed Bed

Zuo-yi Yan, Cheng Lin, and Qi Ruan

Dept. of Chemical Engineering, Fuzhou University, Fuzhou 350108, Fujian, P.R. China

DOI 10.1002/aic.14449

Published online April 4, 2014 in Wiley Online Library (wileyonlinelibrary.com)

*To do further research on the mass-transfer mechanism in rotating packed bed (RPB), dynamics of droplets in a RPB are studied by an analytical approach combined with a series of laboratory measurements. Based on the results of the fluid dynamics, mathematical models of mass-transfer coefficient and mass-transfer process in RPB are proposed, respectively. Mass-transfer experiments in RPB are also carried out using ethanol–water solution. By comparison, the results of simulation agree well with that of the experiment, which demonstrate that both hydrodynamic model and mass-transfer models can better describe the real conditions of RPB. © 2014 American Institute of Chemical Engineers AIChE J, 60: 2705–2723, 2014*

**Keywords:** rotating packed bed, mass-transfer coefficient, model, experiment

## Introduction

Rotating packed bed (RPB), has been widely applied in the chemical process industries, especially in relating to gas–liquid mass-transfer and heat-transfer processes, such as distillation, absorption, and extraction operation and so forth.<sup>1–8</sup> Research results from Dipendu,<sup>6</sup> Kelleher and Fair,<sup>7</sup> and Lin et al.<sup>8</sup> show that the two-phase flow fluid interface and mass-transfer coefficient are greatly enhanced by RPB. This is due to the larger centrifugal acceleration under RPB operation and thinner films and tiny droplets are produced. Therefore, many researchers have focused on the micromorphology of liquid in RPB. Burns and Ramshaw<sup>9</sup> and Zhang et al.<sup>10,11</sup> observed the state of the liquid flow in the RPB using the high-speed stroboscopic photography, and the results show that the liquid in RPB exists in the form of film flow (on the surface of the packings), liquid particles (droplets and filaments in the space among the packings) when the rotor speed is larger than 600 rpm. The size of the liquid film and droplets are very small. The magnitude of the thickness of the liquid film is about  $10^{-6}$ – $10^{-5}$  m and the magnitude of the diameter of the droplets is about  $10^{-5}$ – $10^{-4}$  m. Some formulas have been proposed to estimate the droplet diameter in RPB by the researches of Mochidat et al.,<sup>12</sup> Friedman et al.,<sup>13</sup> and Chen and Zeng.<sup>14</sup> However, the real condition of the droplets behaviors in RPB is very complicated because it involves some complex processes such as droplet–droplet collisions, droplet–packing collisions and so forth. As the droplets behaviors deep inside the random packings are difficult to be captured, these processes have not been studied yet.

In our previous works,<sup>15,16</sup> a novel experimental method was proposed to investigate the fluid flow inside the random packings in RPB. The mathematical model for gas–liquid two-phase flow in RPB was also established based on the experimental results. The distribution of the gas–liquid two-phase flow field, the pressure drop, the liquid film thickness, the proportion of the turbulent flow in the liquid film, and some other complex hydrodynamic characteristics in RPB have been calculated by the mathematical model. These hydrodynamic characteristics have a close relationship with the mass-transfer coefficient in RPB which has not been studied yet.

Therefore, to do further research on the mass-transfer mechanism in RPB, dynamics of droplets in a RPB will be studied by an analytical approach combined with a series of laboratory measurements. Based on the results of the fluid dynamics, mathematical models of mass-transfer coefficient and mass-transfer process in RPB will be proposed, respectively. Finally, the results of the simulation will be compared with that of experiments.

## Experimental Setup

Figure 1 shows a simplified schematic diagram of experimental procedure which mainly consists of a RPB, a reboiler, a condenser, and an electromotor. The electromotor drives the RPB packed with triangular spiral packings to rotate with high speed. The details of the RPB and the physical properties of the triangular spiral packings are listed in Table 1. At the beginning, the feeding mixture of ethanol and water is filled in the reboiler, and heated, for a while, then the vapor rises from the reboiler through the gas import into the outer edge of the packed bed. Vapor travels inward from the outer edge of the rotor by the pressure driving force, contacting with liquid countercurrently to transfer heat and mass, and leaves the rotor at the inner edge. Vapor from RPB is condensed into a condensate against cooling water in overhead condenser. The condensate (liquid) returns to RPB

Correspondence concerning this article should be addressed to C. Lin at enjoy@fzu.edu.cn or hys@fzu.edu.cn.

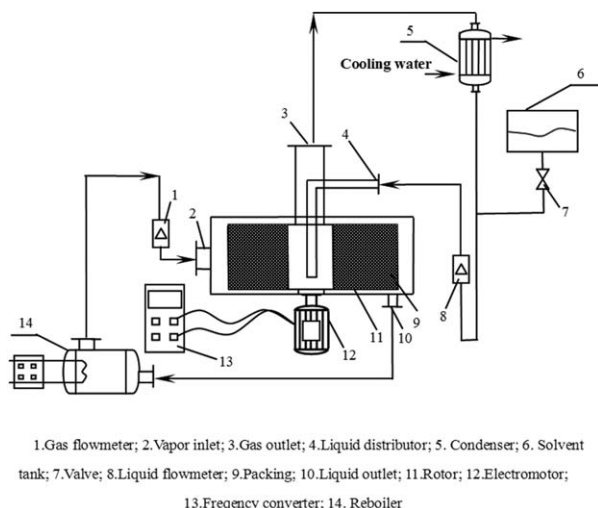


**Figure 1. Experimental setup.**

as full reflux operation. The liquid is pumped into the inner edge of the rotor via a distributor. Inside the bed, the liquid moves outward through the packings because of the centrifugal force action. The liquid is then splashed onto the stationary housing and is collected at the bottom and flows into the reboiler. The equipment is designed for separating the ethanol–water mixture. However, water–ethanol is an azeotropic mixture and the maximum ethanol concentration is about 95% by distillation. Therefore, ethylene glycol is used as extracting agent and the extractive distillation is proposed to get the higher ethanol concentration.

1. Distillation: The ethanol concentration of feeding mixture is 30%. Valve 7 is closed. The liquid flow rates are controlled by adjusting the heating power of reboiler.

2. Extractive distillation: The ethanol concentration of feeding mixture is 95% and the solvent ratios are controlled by adjusting valve clearance.

## Model Description

The mass transfer of the gas–liquid two-phase flow can be described as follows:

At time 0: One part of the liquid travels as a thin film flow on packings surface, whereas the other part travels as flying particles (droplets and filaments) in the space among packings. All spaces are covered with gas.

During  $0-\Delta t$ : The liquid particles (droplets and filaments) pass through the space among packings and the liquid film moves along the solid surface. The liquid film travels the distance of  $\Delta l$  without any interference along the liquid trajectories. The collisions happen between some liquid droplets and the satellite droplets are produced. Gas–liquid film mass-transfer and gas–liquid droplets mass transfer occur at the same time. Two-phase flow fluid interface equals to the surface area of all droplets and the exposed area of all liquid film.

At time  $\Delta t$ : The liquid particle (droplets and filaments) approaches the solid surface and reclothes the film on the packings surface and the other part of the liquid re-enters the space among the packings.

Above steps are repeated until the liquid is thrown out of the RPB.

According to above analysis, the mass balance equation for the light component in the RPB during  $r-r+\Delta l$  can be obtained by

Liquid

$$-D_{AB}^L A_L \frac{\partial^2 x}{\partial r^2} + L \frac{\partial x}{\partial r} + H_0 A_L \frac{\partial x}{\partial t} + K_L a_{LG} (x - x^*) / \Delta l = 0 \quad (1)$$

Gas

$$D_{AB}^G A_V \frac{\partial^2 y}{\partial r^2} + (G + 2\pi h \varepsilon D_{AB}^G) \frac{\partial y}{\partial r} - H'_0 A_V \frac{\partial y}{\partial t} + K_L a_{LG} (x - x^*) / \Delta l = 0 \quad (2)$$

where  $x$  is the mass fraction of ethanol in the liquid,  $y$  is the mass fraction of ethanol in the gas,  $L$  is the flow rate of mixed solution,  $G$  is the flow rate of steam,  $H_0$  is the liquid holdup per unit volume,  $H'_0$  is the gas holdup per unit volume,  $h$  is the height of the bed,  $\varepsilon$  is the porosity of packings,  $A_L$  is the passing section of the liquid flow,  $A_V$  is the passing section of the gas flow,  $K_L$  is the overall mass-transfer coefficient of the liquid, and  $a_{LG}$  is the two-phase flow fluid interface between  $r$  and  $r + \Delta l$ .

Obviously,  $a_{LG}$  and  $K_L$  have a close relationship with the fluid dynamics in RPB. For example, the fluid interface of a single flying droplet is usually considered to be the value of its surface area, however, the surface area is increasing largely when droplet–droplet collision happen (satellite droplets may be produced). In addition,  $K_L$  is also very different between the single flying droplet and droplet–droplet collision. Therefore, dynamics of droplets and mass-transfer coefficient in RPB will be studied, respectively.

## Dynamics of Droplets in RPB

Figures 2 and 3 show the liquid trajectories which are obtained by the novel method mentioned in our previous work.<sup>15,16</sup> As shown in Figure 2, it is found that the trajectories consist of many confluences (the liquid trajectories are shown at higher magnification). This means the liquid has intersecting trajectories and the collisions happen. As shown in Figure 3, it is found that the trajectories consist of many short lines and nodes, which reflect that the frequency of the hitting between liquid droplets and packings is very high. In addition, the motion of the liquid droplets in the packing space involves the deformation and breakup of liquid droplets in two-phase flow. These processes will be studied in this section, respectively.

### Droplet–droplet collisions in RPB

Sommerfeld,<sup>17</sup> O'Rourke,<sup>18</sup> Kim et al.,<sup>19</sup> Ashgriz and Poo,<sup>20</sup> Brazier-Smith et al.,<sup>21</sup> Qian and Law,<sup>22</sup> and

**Table 1. Details of the Rotating Packed Bed and the Physical Properties of the Triangular Spiral Packings**

Details of the Rotating Packed Bed		Physical Properties of the Packing	
Outer diameter	300 (mm)	Dimension of the packing	$2 \times 2$ (mm)
Inner diameter	100 (mm)	Specific surface area	2500 (m <sup>2</sup> /m <sup>3</sup> )
Axial length of the rotor	30 (mm)	Packing porosity	0.84
Radial length of the rotor	100 (mm)	Packing density	1160 (kg/m <sup>3</sup> )

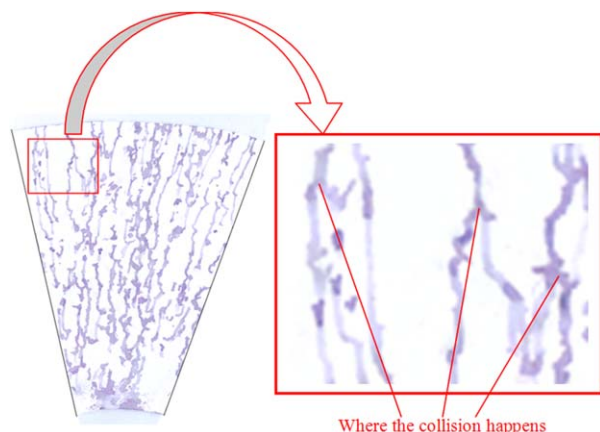


**Figure 2. The intersecting liquid trajectories are shown at higher magnification.**

[Color figure can be viewed in the online issue, which is available at [wileyonlinelibrary.com](http://wileyonlinelibrary.com).]

Tennison et al.<sup>23</sup> and so forth, have already studied the droplet–droplet collisions in gravity fields. However, there are hypergravity fields in RPB and the space among the packings is limited. These make the droplet–droplet collisions in RPB have some different outcomes. For example, in gravity fields, Sommerfeld<sup>17</sup> and O'Rourke<sup>18</sup> have already developed some models to predict the collision probability, however, all above models cannot accurately predict the collision probability in RPB according to our calculation results. Therefore, the distinct regularity and characteristic of the droplet–droplet collisions in RPB are listed as following expressions:

1. The collision probability.  $P_d$  is defined as the collision frequency per unit radial length and per unit liquid trajectory. According to the experiment method mentioned in our previous works,<sup>15,16</sup> all liquid trajectories can be captured by the plate on the outer edge.  $P_d$  is supposed to be a fixed value under a certain operational conditions (liquid flow rate, rotor speed) in RPB. A small radial length  $\Delta l_d$  is taken near the outer edge of the flabellate paper and the area between two blue dotted lines is defined as statistic region which is shown in Figure 4, then the collision frequency per unit radial length and per unit liquid trajectory,  $P_d$ , can be obtained by

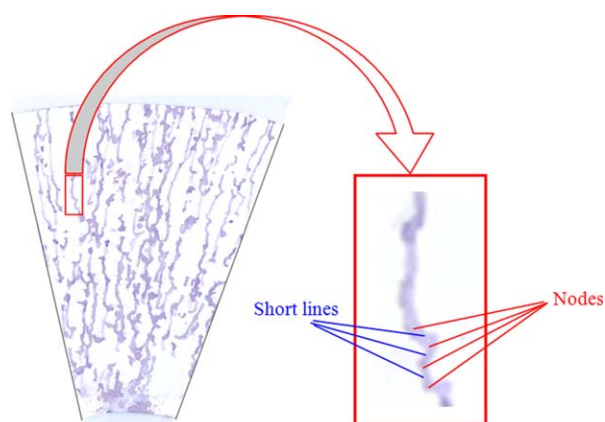


**Figure 3. The nodes and short lines of the liquid trajectories are shown at higher magnification.**

[Color figure can be viewed in the online issue, which is available at [wileyonlinelibrary.com](http://wileyonlinelibrary.com).]

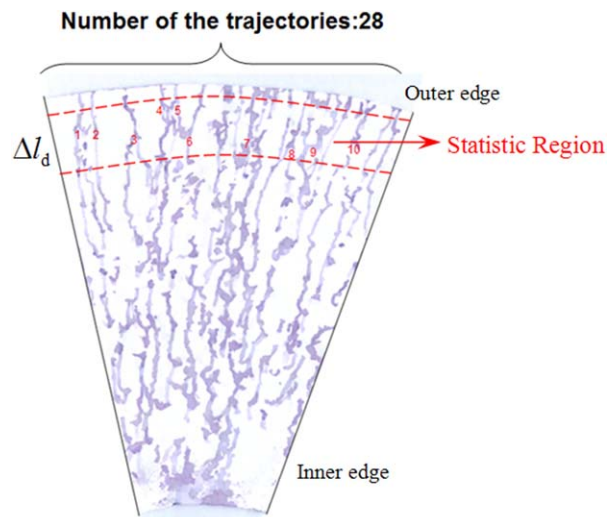


**Figure 4. Statistic region is taken in the region near the outer edge of the flabellate paper.**

[Color figure can be viewed in the online issue, which is available at [wileyonlinelibrary.com](http://wileyonlinelibrary.com).]

$$P_d = \frac{N_d}{\Delta l_d N_w} \quad (3)$$

where  $N_d$  is the number of the intersectional liquid trajectories in statistic region.  $N_w$  is the whole number of liquid trajectories in statistic region.

2. Different collision outcomes. As shown in Figure 5, one collision outcome is separation collision which can be divided further into two types: off-center separation (reflexive separation) or near head-on separation (stretching separation). In this situation, two droplets impact and then separate into two or more droplets. In another words, it is more likely to produce some satellite droplets when the separation collision happens. If these satellite droplets are captured by the packings, it will leave the big mark on the paper (shown by the red arrow in Figure 5). Second possible collision outcome is coalescence, and detailed process of the collision is shown in Figure 6. In this situation, two droplets combine and become a single droplet. It is reflected on the paper is that two liquid trajectories are combined into one. Similarly, as shown in Figure 7, third possible collision outcome is bouncing.

3. Droplets velocity. In RPB, one part of the droplets comes from the space of the inner packings (see Figure 8), the other part of the droplets comes from the liquid film

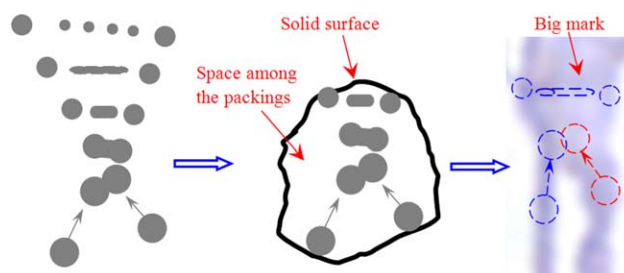


**Figure 5. The possible collision outcome is separation collision in RPB.**

[Color figure can be viewed in the online issue, which is available at [wileyonlinelibrary.com](http://wileyonlinelibrary.com).]



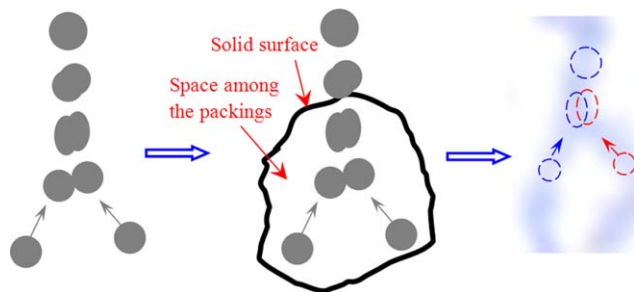


**Figure 6. The possible collision outcome is coalescence in RPB.**

[Color figure can be viewed in the online issue, which is available at [wileyonlinelibrary.com](http://wileyonlinelibrary.com).]

flow which is thrown out from the packing surface because of the strong centrifugal force. As shown in Figure 8, the boundary layer develops from the position A when the liquid film travels in a very short distance AC on the surface of solid packings. The liquid is thrown away at the position C and the droplets are formed. In our previous works in Ref. 16, the velocity distribution of the liquid film flow  $U_{x,z}$ , and the liquid film thickness  $\delta_L$  has already been obtained. In this situation,  $U_{d,r}^i$  is introduced to describe the velocity of the liquid droplets at the radial position of  $r$ . As  $i = 1$ ,  $U_{d,r}^1$  represents the first part droplets at the radial position of  $r$  (comes from the space of the inner packing). As  $i = 2$ ,  $U_{d,r}^2$  represents the velocity of the second part droplets at the radial position of  $r$  (comes from the liquid film flow which is thrown out from the packing surface).  $U_{d,r}^i$  can be obtained by

$$U_{d,r}^i \approx \begin{cases} U_{r\infty}, i=1 \\ U_{d,r} = \frac{\int_0^{\delta_L} \frac{2U_{r\infty}}{\delta_{L1}} \left( z - \frac{z^2}{2\delta_L} \right) dz}{\delta_L L_c}, i=2 \end{cases} \quad (4)$$

where  $U_{r\infty}$  is the velocity of the undisturbed liquid flow at the radial position of  $r$  (see Ref. 16). The velocity of the liquid droplets after collision,  $U_{d,r}^i$ , can be obtained by energy and momentum conservation which is proposed by Brazier-Smith et al.<sup>21</sup>

4. Judge criteria. Munnannur and Reitz<sup>24</sup> have already developed a predictive collision model for the formation of satellite droplets which come from the breakup of the ligament. However, as the space among packings in RPB is very limited, one should consider whether the ligament is directly

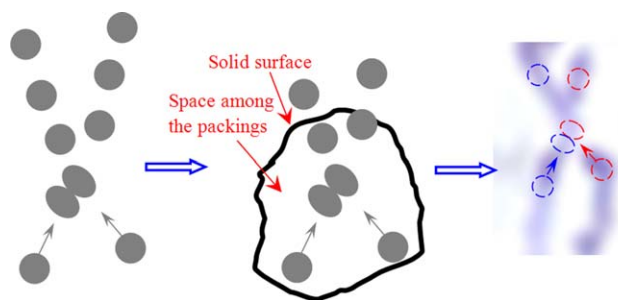


**Figure 7. The possible collision outcome is bouncing in RPB.**

[Color figure can be viewed in the online issue, which is available at [wileyonlinelibrary.com](http://wileyonlinelibrary.com).]

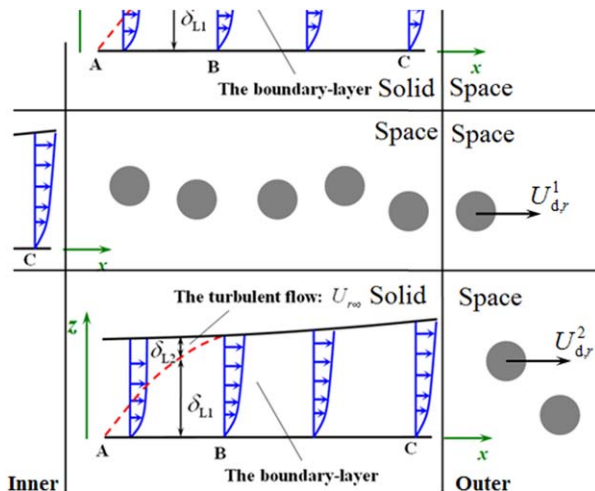


**Figure 8. Droplets come from the liquid film flow.**

[Color figure can be viewed in the online issue, which is available at [wileyonlinelibrary.com](http://wileyonlinelibrary.com).]

captured by the packings. Therefore,  $t_{d,r}$  is introduced to describe the time of the breakup of the ligament. If the satellite droplets is produced then

$$t_{d,r} = \frac{l_1}{U_{d,r}^i} \quad (5)$$

where  $l_1$  is the flying distance of the liquid ligament in the space among packings after collision.  $U_{d,r}^i$  is the velocity of the liquid ligament after collision at the radial position of  $r$ . Combined with the conclusion of the Munnannur and Reitz,<sup>24</sup> the outcomes of the liquid droplets collision for the near head-on separation (stretching separation) can be described as:

1.  $C_{VS} < 0$ ,  $N_{sat} = 0$  (no ligament or satellite droplet is produced);
2.  $C_{VS} \geq 0$ ,  $T \leq 2$ ,  $N_{sat} = 1$  (ligament contraction into a single satellite);
3.  $t_{d,r} < \frac{l_1}{U_{d,r}^i}$ ,  $C_{VS} \geq 0$ ,  $T > 2$ ,  $N_{sat} > 1$  (ligament contraction into several satellite droplets);
4.  $t_{d,r} > \frac{l_1}{U_{d,r}^i}$ ,  $C_{VS} \geq 0$ ,  $T > 2$ ,  $N_{sat} = 0$  (ligament is captured by the packings and no satellite droplet is produced)

Similarly, the outcomes of the liquid droplets collision for the off-center separation (reflexive separation) can be described as:

1.  $T \leq 3$ ,  $N_{sat} = 1$  (ligament contraction into a single satellite);
2.  $t_{d,r} < \frac{l_1}{U_{d,r}^i}$ ,  $T > 2$ ,  $N_{sat} > 1$  (ligament contraction into several satellite droplets);
3.  $t_{d,r} > \frac{l_1}{U_{d,r}^i}$ ,  $T > 2$ ,  $N_{sat} = 1$  (ligament is captured by the packing and no satellite droplet is produced).

In above judge criteria,  $C_{VS}$  is the separation volume coefficient.  $N_{sat}$  is the number of satellite droplets.  $T$  is the time scale. The calculation process of  $C_{VS}$ ,  $N_{sat}$ ,  $T$ , and the diameter of the satellite droplets ( $d_{sat}$ ) are described in detail in the researches of Munnannur and Reitz.<sup>24</sup>

### Droplet-packing collisions in RPB

The collision process between droplets and packings in RPB can be deemed as a droplet-wall collision. The possible outcomes of droplet-wall collision are listed as follows:

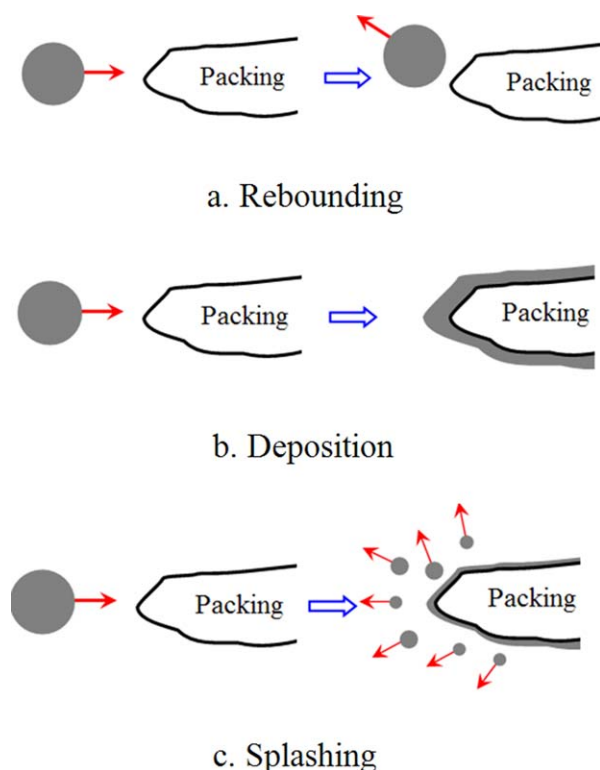


**Figure 9. The possible outcomes of droplet impingement on a solid packing surface.**

[Color figure can be viewed in the online issue, which is available at [wileyonlinelibrary.com](http://wileyonlinelibrary.com).]

1. The droplet rebounds after collision (see Figure 9a).
2. The droplet deposits on the surface and form a liquid film (see Figure 9b).
3. The droplet splashes and secondary droplets are formed (see Figure 9c).

Many researchers such as Escure et al.,<sup>25</sup> Zhang and Osman,<sup>26</sup> Mundo et al.,<sup>27</sup> and Chandra and Avedisian<sup>28</sup> have already studied the basic mechanisms of droplet-wall collisions in the gravity field. Combined with experimental data, the judge criteria of the collision (splashing or deposition) is obtained by Mundo et al.,<sup>27,29</sup> Lavergne and Platet.<sup>30</sup> Escure et al.<sup>25</sup> complemented the judge criteria of Mundo et al.<sup>27</sup> and the droplet behavior after collision (on a dry cold surface or slightly wet) is

1.  $We_{LS}^{0.5} Re_{LS}^{0.25} \leq 3$ , bounce;
2.  $3 < We_{LS}^{0.5} Re_{LS}^{0.25} \leq 57.7$ , deposition;
3.  $We_{LS}^{0.5} Re_{LS}^{0.25} > 57.7$ , splashing.

The values of  $We_{LS}$  and  $Re_{LS}$  can be easily calculated which are described in detail in the researches of Escure et al.<sup>25</sup> The velocity of liquid droplets can be calculated by Eq. 4. The space among the packings in RPB is very limited and the outcomes may be very different from Ref. 25 if the splashing or bounce happened. However, according to our calculation results and the experiment results, there is only one result for droplet-wall collisions in RPB: deposition (see results and discussion in this article). Therefore, it is no need to propose the judge criteria for the children droplets here.

#### Deformation and breakup of liquid droplets in RPB

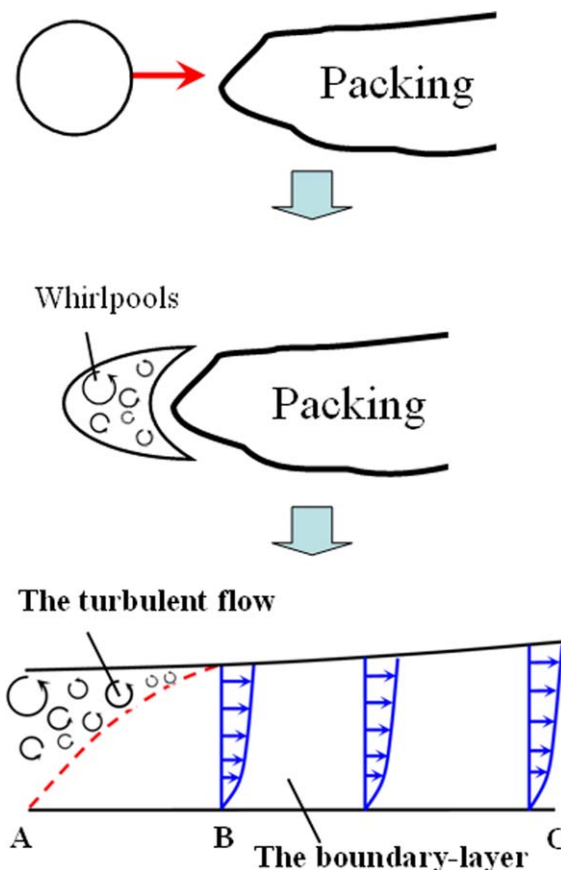
Many researchers (such as Pilch and Erdman,<sup>31</sup> Hsiang and Faeth,<sup>32–34</sup> and Theofanous et al.,<sup>35</sup> etc.) focused on the

basic mechanisms of the deformation and breakup process of liquid droplet in gas–liquid two-phase flow, and four different outcomes of the deformation and breakup of liquid droplet in gas–liquid two-phase flow have been proposed in gravity field (see Refs. 31–35): (1) Vibrational mode. (2) Bag breakup. (3) Stretching and thinning breakup. (4) Catastrophic breakup. The Weber number  $We_{LG}$  is universally regarded as a judge criterion for the droplet deformation and breakup.

In RPB, the Weber number at any position  $(r, z, \theta)$ ,  $We_{LG,r,z,\theta}$ , can be obtained by

$$We_{LG,r,z,\theta} = \frac{\rho_G |U_{d,r}^i - V_{r,z,\theta}|^2 d_L}{\sigma_L} \quad (6)$$

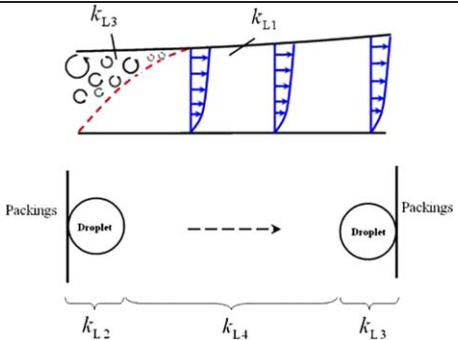
where  $|U_{d,r}^i - V_{r,z,\theta}|$  is the relative velocity between droplet and gas.  $V_{r,z,\theta}$  is the velocity of the gas at any position  $(r, z, \theta)$  in RPB. According to our previous works in Ref. 16, when the gas (single phase) passes through the packings, the packings constitute a group of complex disorderly channels (the wall of the channel is structured by the random packings). To quantify the dimensions of these disorderly channels, an element is taken along the radial direction. As  $dr$  approach zero, the channel can be described as a virtual tube. Furthermore, Zheng et al.,<sup>36</sup> Sandilya et al.,<sup>37</sup> Liu et al.,<sup>38</sup> and Rao et al.<sup>39</sup> studied the angular velocity of gas in RPB and found that the gas flows are circular with very small velocity differences between the gas flows and the packings are observed. Therefore, the distribution of the gas velocity is of axial symmetry.  $V_{r,z,\theta}$  has nothing to do with  $\theta$ . The velocity distribution of the gas in the virtual



**Figure 10. The liquid film flow on the packing surface.**

[Color figure can be viewed in the online issue, which is available at [wileyonlinelibrary.com](http://wileyonlinelibrary.com).]

**Table 2. Different Mass-Transfer Coefficients**

$k_{L1}$	Mass-transfer coefficient of the liquid boundary-layer	
$k_{L2}$	Mass-transfer coefficient of the drop formation	
$k_{L3}$	Mass-transfer coefficient of the droplet approaching the solid surface	
$k_{L4}$	Mass-transfer coefficient for the droplet flying through the space among the packings	

tube can be used to approximate the real gas velocity distribution in the packing space using the  $1/n$  law

$$V_{r,z,\theta} = V_{r,\max} \left( \frac{2(z-id_e)}{d_e} \right)^{1/n} \quad id_e \leq z \leq \left( i + \frac{1}{2} \right) d_e, \quad i=0, 1, 2, 3 \dots \quad (7)$$

$$V_{r,z,\theta} = V_{r,\max} \left( 1 - \frac{2(z-id_e)}{d_e} \right)^{1/n} \quad \left( i + \frac{1}{2} \right) d_e \leq z \leq (i+1)d_e, \quad i=0, 1, 2, 3 \dots \quad (8)$$

### Mass-Transfer Coefficients in RPBs

According to hydrodynamic results, there are different mass-transfer coefficients based on different liquid flow forms. First, as shown in Figure 10, the mass-transfer coefficient in segment AB is very different from that in segment BC. Second, the mass-transfer coefficient of the droplet forming and the droplet approaching the solid surface are very different from that of the single droplet flying through the space. Finally, the mass-transfer coefficient of droplet-droplet collisions is also very different from that of single flying droplets. Therefore, these different mass-transfer coefficients are defined as  $k_{L1}$ – $k_{L4}$ , which are listed in Table 2.

As shown in Figure 10, suppose that  $Sc > 1$  and the development of the concentration boundary layer in the liquid film flow is shown by the dotted line in Figure 11, the mass balance equation for the component A by Eq. 9

$$\frac{Dc_A}{Dt} + c_A \nabla \cdot U + \nabla \cdot J_A - r_A = 0 \quad (9)$$

where  $c_A$  is the mass concentration of the component A;  $U$  is the velocity of the liquid in the irrigated bed;  $r_A$  is the rate of the formation of the component A in the chemical reactions, and  $r_A = 0$  without any chemical reaction; the liquid diffusion coefficient,  $D_{AB}^L$  of a component A in solution in B, which is a measure of its diffusive mobility is then defined as the ratio of its flux  $J_A$  to its concentration gradient

$$J_A = -D_{AB}^L \nabla c_A \quad (10)$$

Under the precondition of incompressible flow without chemical reaction, Eq. 9 can be simplified by

$$\frac{Dc_A}{Dt} = D_{AB}^L \nabla^2 c_A \quad (11)$$

The equation of the continuity of the boundary layer flow for liquid is

$$\nabla \cdot U = 0 \quad (12)$$

The width of the liquid trajectories is not changed along the radial direction

$$U_y = 0 \quad (\text{boundary layer}) \quad (13)$$

The value of  $D_{AB}^L \frac{\partial^2 c_A}{\partial x^2}$  is one magnitude less than other items and it can be neglected. By solving the simultaneous equations (9)–(13), Eq. 14 can be obtained

$$\frac{\partial}{\partial x} \left( \int_0^{\delta_{L1}} c_A U_x dz \right) - \frac{\partial}{\partial x} \left( \int_0^{\delta_{L1}} c_{A\infty} U_x dz \right) = D_{AB}^L \left( \frac{\partial c_A}{\partial y} \right)_{y=0} \quad (14)$$

The concentration distribution in the concentration boundary layer is also supposed as parabola

$$\frac{c_A - c_{As}}{c_{A\infty} - c_{As}} = \frac{1}{2} \left( \frac{z}{\delta_D} \right) - \left( \frac{z}{\delta_D} \right)^2 \quad (15)$$

Suppose that the ratio of concentration boundary layer to velocity boundary layer is  $\xi$ , which can be obtained by

$$\xi = \frac{\delta_D}{\delta_{L1}} \quad (16)$$

According to our previous works in Ref. 16,  $\delta_{L1}$  represents the velocity boundary layer between  $r \sim (r + \Delta l)$  and is obtained by

$$\delta_{L1} = \left( \frac{1}{U_{r\infty}^{19}} \left( \int \frac{30\mu}{\rho_L} U_{r\infty}^{18} dr + c_2 \right) \right)^{0.5} \quad (17)$$

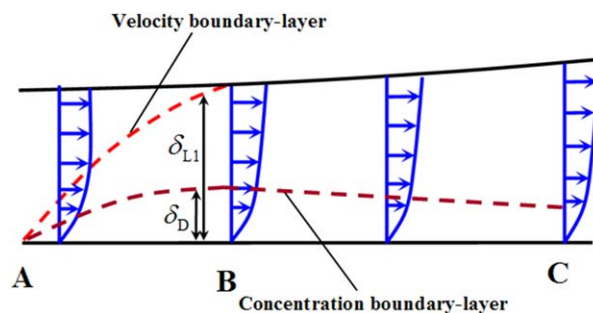


**Figure 11. The development of the concentration boundary layer in the liquid film flow.**

[Color figure can be viewed in the online issue, which is available at [wileyonlinelibrary.com](http://wileyonlinelibrary.com).]

As distance for the liquid film flow in one time is very short, the value of  $U_{r\infty}$  is supposed to be a constant during  $\Delta l$ . In this situation, Eq. 17 can be simplified as

$$\delta_{L1} = \left[ \frac{1}{U_{r\infty}} \frac{30\mu}{\rho_L} (r+c_3) \right]^{0.5} \quad (18)$$

According to our examination, the calculation result of Eq. 18 is a little bigger than that of Eq. 17, however, they are basically in the same magnitude. Suppose that the thickness of the velocity boundary layer is zero in position A ( $r=r_0$ ), Eq. 16 can be rewritten as

$$\zeta = \frac{\delta_D}{\left[ \frac{1}{U_{r\infty}} \frac{30\mu}{\rho_L} (r+r_0) \right]^{0.5}} \quad (19)$$

By solving the simultaneous equations (11)–(19), Eq. 20 can be obtained

$$\zeta = \frac{\delta_D}{\delta_{L1}} = \left[ \frac{4D_{AB}^L \rho_L - c_4 |r-r_0|^{-\frac{3}{4}}}{5\mu} \right]^{\frac{1}{3}} \quad (20)$$

Suppose that the development of the concentration boundary layer is simultaneous with the development of the velocity boundary layer, Eq. 20 can be written as

$$\zeta = \frac{\delta_D}{\delta_{L1}} = \left[ \frac{4D_{AB}^L \rho_L}{5\mu} \right]^{\frac{1}{3}} \quad (21)$$

The mass-transfer coefficient for the liquid film flow in segment BC,  $k_{L1}$ , can be obtained by

$$k_{L1} = \frac{D_{AB}^L}{\Delta c_A} \left( \frac{\partial c_A}{\partial n} \right)_{n=0} = \frac{D_{AB}^L}{c_{As} - c_{A\infty}} \left( \frac{\partial c_A}{\partial n} \right)_{n=0} = \frac{2D_{AB}^L}{\zeta \delta_{L1}} \quad (22)$$

Substituting Eq. 21 into Eq. 22 yields

$$k_{L1} = \frac{2D_{AB}^L}{\delta_{L1}} \left( \frac{4D_{AB}^L \rho_L}{5\mu} \right)^{-\frac{1}{3}} = 2.154 \frac{D_{AB}^L}{\delta_{L1}} (Sc)^{\frac{1}{3}} \quad (23)$$

$k_{L1}$  is proportional to  $(Sc)^{\frac{1}{3}}$ .  $k_{L1}$  is the mass-transfer coefficient for the liquid film flow in segment BC.  $\chi_1$  is defined as the proportion of the laminar flow in the whole liquid flow

$$\chi_1 = (1-\beta) \frac{|BC|}{|AC|} \quad (24)$$

The solution method of  $\frac{|BC|}{|AC|}$  is introduced in our previous works (see Ref. 16).

The oscillation and distortion occur in the droplets when the liquid droplets are approaching the solid surface. There are self-circulating flow and abundant whirlpools in the droplet signifying violent turbulence when the liquid droplets just arrive on the solid surface (shown in AB segment in Figure 10). Much experimental effort has been made to investigate the mass-transfer rate during the droplet formation.<sup>40–45</sup> Different experimental approaches have been established such as extrapolation methods to zero formation time or zero column height, the formation-collapse technique where the droplet is withdrawn after formation by the same nozzle, or using short column heights (see Refs. 46–48). Based on the penetration theory by Higbie,<sup>49</sup> Popovich et al.<sup>43</sup> showed that the total transferred mass  $M_A$  calculated by these models can be described with Eq. 25 if the spherical droplet grows uniformly with time

$$M_A = \text{const} \cdot d_m^2 \Delta c_A \sqrt{t_f \pi D_{AB}^L} \quad (25)$$

where  $d_m$  is the droplet diameter,  $t_f$  is the drop formation time, and  $\Delta c_A$  is the concentration difference between the initial solution concentration  $c_{A,0}$  inside the drop and the equilibrium concentration in the drop for  $t \rightarrow \infty$ . The constant varies according to the different assumptions used in the models between the lowest value 6/7 (Licht and Pansing<sup>45</sup>) and 24/7 (Heertjes et al.<sup>41,42</sup>). In this situation, the mass-transfer coefficient of the drop formation,  $k_{L2}$ , can be obtained by

$$k_{L2} = \frac{M_A}{t_f a_d \Delta c_A} \quad (26)$$

where  $a_d$  is the mass-transfer interface, which equals to surface area of liquid droplet

$$a_d = 4\pi (d_m/2)^2 \quad (27)$$

$t_f$  can be obtained approximately by

$$t_f \approx \frac{d_m}{U_{d,r}^i} \quad (28)$$

$U_{d,r}^i$  is the velocity of the liquid droplets before collision at the radial position of  $r$ .  $\chi_2$  is defined as the proportion of the drop formation in the whole liquid flow, and it can be obtained by

$$\chi_2 = \beta \frac{d_m}{\Delta l} \quad (29)$$

The process of the droplet approaching the solid surface is deemed as the reverse process of droplet forming, then

$$k_{L3} = k_{L2}, \chi_3 = \chi_2 \quad (30)$$

where  $k_{L3}$  is the mass-transfer coefficient of the droplet approaching the solid surface.  $\chi_3$  is the proportion of the droplet approaching the solid surface in the whole liquid flow.

$k_{L4}$  is defined as the mass-transfer coefficient for the droplet flying through the space among the packings. As the value of  $We_{LG}$  is very low in RPB (the magnitude of  $We_{LG}$  is about  $10^{-2}$ ), it is reasonable to consider that the droplet only is deformed and does not have the ability to break up when it is flying through the space among the packings. According to Refs. 50–52,  $k_{L4}$  can be obtained by

$$k_{L4} = \frac{d_m}{6t} \ln \left( \frac{1}{\Delta'} \right) \quad (31)$$

where  $\Delta' \equiv \frac{6}{\pi^2} \sum_{n=1}^{\infty} \frac{1}{n^2} e^{-4n^2 \pi^2 Fo}$ .  $Fo$  is Fourier number for the mass transfer, and can be obtained by

$$Fo \equiv D_{AB}^L t / (d_m/2)^2 \quad (32)$$

However, during this process, droplet–droplet collisions may occur. If droplet–droplet collisions occur, the possible outcomes are: separation, bouncing, and coalescence. If the separation collision or the coalescence collision occurs, there exist obviously big momentum exchange and mass exchange among droplets. Bouncing collision is something different from separation collision and coalescence collision. If the bouncing collision happens, two droplets do not actually contact each other due to the layer of gas trapped in between them in this situation. It means the bouncing collision is



when a gas film prevents contact between the droplet surfaces, causing the droplets to bounce apart. However, when two droplets approach each other, the oscillation and distortion occur. Therefore, either way, the process of droplet–droplet collisions increases the surface renewal greatly and reduces the mass-transfer resistance near the gas–liquid surface. In this situation, the collision probability should be obtained in advance. The collision probability can be calculated by the probability of the intersecting trajectories in RPB. If droplet–droplet collisions occur, mass-transfer coefficients for different outcomes (separation, bouncing, and coalescence) are deemed to be in the same magnitude in this article. Therefore, in this situation,  $k_{L4}$  is deemed to be equal to the mass-transfer coefficient for satellite droplets forming. The mass-transfer coefficient for satellite droplets forming is similar to that for the single droplet forming which can be obtained by Eq. 25.

Zheng et al.,<sup>36</sup> Sandilya et al.,<sup>37</sup> Liu et al.,<sup>38</sup> and Rao et al.<sup>39</sup> studied the angular velocity of gas in the RPB and found that the gas goes round and round in RPB and is keeping pace with the packings all the time. This assertion is supported by the work of Liu et al.<sup>38</sup> These observations indicate that the circumferential force exerted by packings counterbalances with Coriolis force, which means that packings do affect on the gas continually. In addition, as the gas passes through the serpentine microchannels which are built by the random packings, the direction and the speed of the gas are always changing. Above two factors indicate that the turbulence extent of the gas is increased effectively when it passes through RPB. Therefore, in our previous works in Ref. 16, the gas velocity distribution in the packings space is approximated using the  $1/n$  law. However, it becomes more complicated in the mass-transfer problem because not all gas channels are wetted by liquid. The liquid in RPB has its distinctive flow characteristics: the liquid travels along the liquid trajectories. Further more, as some of the liquid travels as film flow and the other travels as flying droplets, the problem becomes much more complicated. Guo<sup>53</sup> and Kang et al.<sup>54</sup> proposed the calculated formula of mass-transfer coefficient in gas phase based on the “Surface renewal” theory

$$k_G = \sqrt{k_s D_{AB}^G (V^2 + \omega^2 r^2)} \quad (33)$$

where  $V$  is the gas velocity in the noninertial reference frame;  $\omega$  is the rotational speed; and  $k_s$  is the fit parameter. The fitted values of  $k_s$  in Refs. 53 and 54 have the same order of magnitude (about  $10^4$ ). In fact, most of gas–liquid mass-transfer systems in industry are mainly controlled by liquid film diffusion because the gas diffusion coefficient is much higher than the liquid’s. Therefore,  $k_G$  may be ignored in most instances.

## Model Solution

### Pseudolinear transform of the mass-transfer driving force

In Eqs. 1 and 2, the item of  $K_{La_{LG}}(x-x^*)/\Delta l$ ,  $A_L$ ,  $A_V$ , and  $H_0$  varies with the radius  $r$ . As  $\Delta l$  is very short,  $A_L$  and  $A_V$  are nearly unchanged

$$A_L \approx \frac{[\pi(r+\Delta l)^2 - \pi r^2] h H_0}{\Delta l} \quad (34)$$

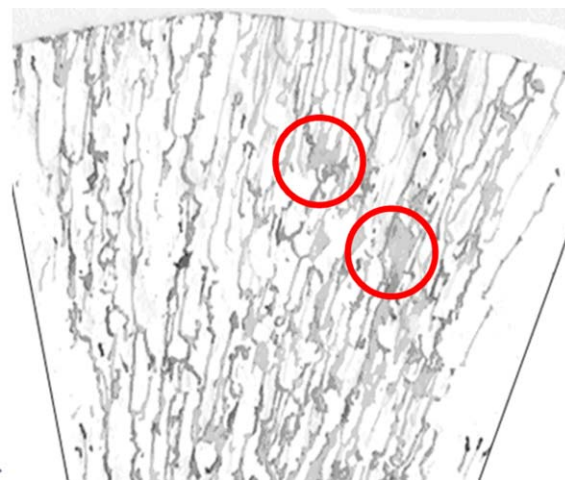


Figure 12. Big marks caused by the “Death Corner.”

[Color figure can be viewed in the online issue, which is available at [wileyonlinelibrary.com](http://wileyonlinelibrary.com).]

$$A_V \approx \frac{2\pi r h \varepsilon + 2\pi(r+\Delta l) h \varepsilon}{2} - \frac{[\pi(r+\Delta l)^2 - \pi r^2] h H_0}{\Delta l} \quad (35)$$

$H_0$  also can be deemed as a constant ( $\Delta l$  is very short). Many researchers (such as Basic and Dudukovic,<sup>55</sup> Burns et al.,<sup>56</sup> Zhou et al.,<sup>57</sup> etc.) have studied the liquid holdup of the RPB using conductance method and many prediction formulas have been proposed. However, their results are of difference, which may be caused by the different type of RPBs. However, most literature showed that the liquid holdup in RPB is about 5%. In fact, according to the number of liquid trajectories obtained in our previous works (Ref. 15), the liquid holdup is much less than the result of Basic and Dudukovic<sup>55</sup> and Zhou et al.<sup>57</sup> Therefore, the liquid holdup may not only consider the liquid trajectories. As shown in Figure 12 (see the red circle), the big mark is caused by the “Dead Corner” which is built by the disorderly and unsystematic packings, which delay the liquid flowing out smoothly. These parts of liquid should be taken into account.

In fact, the item of  $K_{La_{LG}}(x-x^*)/\Delta l$  can be deemed as the mass-transfer driving force which varies with the radius  $r$ . However, as  $\Delta l$  is very short, the mass fraction of ethanol  $x$  changes small in  $\Delta l$ . Thus, the mass-transfer driving force in  $\Delta l$  can be supposed to be a pseudolinear function of radius (shown in Figure 13), that is

$$K_{La_{LG}}(x-x^*)/\Delta l = \varphi(r) \approx a_f r + b_f \quad (36)$$

where  $a_f$  and  $b_f$  are constants. Obviously,  $a_f$  and  $b_f$  have a close relationship with  $k_L$  and  $a_{LG}$ .

### Combination of $k_L$ ( $a_{LG}$ )

Different liquid flow forms determine different mass-transfer coefficients and two-phase flow fluid interface.  $k_L$  can be obtained by mixing different mass-transfer coefficients in a certain ratio

$$k_L = \sum \chi_i k_{Li} \quad (37)$$

$a_{LG}$  is defined as the two-phase flow fluid interface, which can be obtained by mixing different  $a_{LGi}$ .

First, the width ( $L_e$ ), the thickness of the liquid film ( $\delta_L$ ), and the proportion of the turbulent flow in the liquid film



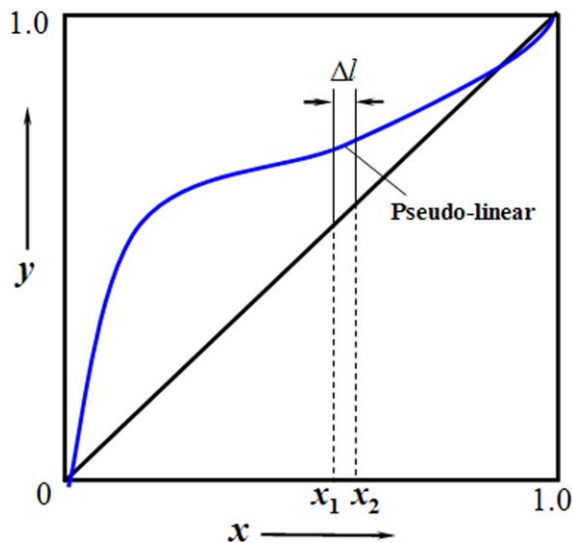


**Figure 13. The mass-transfer driving force in  $\Delta l$  is a pseudolinear function of radius.**

[Color figure can be viewed in the online issue, which is available at [wileyonlinelibrary.com](http://wileyonlinelibrary.com).]

flow have already been calculated in our previous works (Refs. 15 and 16). The liquid holdup can be divided into two parts: One part of the liquid travels as a thin film flow on the packings surface, whereas the other part travels as flying particles (droplets and filaments) in the space among the packings. As the size of the liquid film, droplets, and filaments are far smaller than the packings', the ratio of the liquid film flow and flying particles depends on the porosity of the packings. The chance for the liquid entering the space among the packings is equal to porosity, that is,  $\beta = \varepsilon$ .  $a_{LG1}$  is defined as the two-phase flow fluid interface for the liquid film flow which can be obtained by

$$a_{LG1} = \frac{(1-\beta)H_0 [\pi(r+\Delta l)^2 - \pi r^2] h}{\bar{\delta}_L} \quad (38)$$

where  $\bar{\delta}_L$  is the average film thickness, which can be obtained by

$$\bar{\delta}_L = \frac{\int_0^{\Delta l} \delta_L dr}{\Delta l} \quad (39)$$

Second,  $n_F$  is defined as the number of the flying droplets before droplet–droplet collision, which can be obtained by

$$n_F = \frac{\beta [\pi(r+\Delta l)^2 - \pi r^2] h H_0}{4/3\pi(d_m/2)^3} \quad (40)$$

where  $d_m$  is the droplet diameter in RPB, which can be obtained by some prediction formulas in Refs. 12–14.

$n_C$  is defined as the number of the droplets that collide during  $r-r+\Delta l$ , which can be obtained by

$$n_C \approx 2n_W P_d \Delta l \quad (41)$$

The position and the velocity of the droplets should be given in advance. The position of the droplets must be any location on the liquid trajectories, therefore, the position of the droplets is initialized using a group of random values in this article. By the droplets behaviors simulation (see Table 3 in this article),

the number and the diameter of satellite droplets ( $n_{sat}$ ,  $d_{sat}$ ), the number and the diameter of end droplets ( $n_{end}$ ,  $d_{end}$ ), the number and the diameter of the bouncing droplets ( $n_{bo}$ ,  $d_{bo}$ ), and the number and the diameter of the coalescence droplets ( $n_{co}$ ,  $d_{co}$ ) can be obtained by simulation. In this situation,  $a_{LG2}$  is defined as the two-phase flow fluid interface for the flying liquid droplets, which can be obtained by

$$a_{LG2} = (n_F - n_C) 4\pi(d_m/2)^2 + n_{sat} 4\pi(d_{sat}/2)^2 + n_{end} 4\pi(d_{end}/2)^2 + n_{bo} 4\pi(d_{bo}/2)^2 + n_{co} 4\pi(d_{co}/2)^2 \quad (42)$$

Finally, as the liquid first enters the entry region, there is a great relative movement between the liquid and the packings along the circumferential direction. The packings are almost wetted by the liquid totally. Therefore,  $a_{LG3}$  is defined as the two-phase flow fluid interface for liquid film flowing in the Entry region.  $a_{LG3}$  can be obtained by

$$a_{LG3} = [\pi(r_1 + l)^2 - \pi r_1^2] h a \quad (43)$$

Besides, the liquid droplets also exist in the space among the packings in the entry region. The ratio of the liquid film flow and flying particles also depends on the packings porosity in the entry region ( $\beta = \varepsilon$ ). As the liquid first enters the entry region, the momentum has not been transferred from the packings to the liquid. In this time, the liquid is mainly displayed that it is cut off into fragments consecutively by the packings because the great relative movement between the liquid and the packings along the circumferential direction. Therefore, droplet–droplet collision is not considered in the entry region.  $a_{LG4}$  is defined as the two-phase flow fluid interface for the liquid droplets in the entry region, which can be obtained by

$$a_{LG4} = \frac{6\beta [\pi(r_1 + l)^2 - \pi r_1^2] h H_0}{d_m} \quad (44)$$

### Theoretical solutions

Supposed the system is stable finally, then

$$\frac{\partial x}{\partial t} = 0, \quad \frac{\partial y}{\partial t} = 0 \quad (45)$$

Eqs. 1 and 2 can be simplified as

Liquid

$$-D_{AB}^L A_L \frac{\partial^2 x}{\partial r^2} + L \frac{\partial x}{\partial r} + \varphi(r) = 0 \quad (46)$$

Gas

$$D_{AB}^G A_V \frac{\partial^2 y}{\partial r^2} + (G + 2\pi h \varepsilon D_{AB}^G) \frac{\partial y}{\partial r} + \varphi(r) = 0 \quad (47)$$

The solution is

$$x = C_1 e^{\frac{L}{A_L D_{AB}^L} r} - \frac{1}{2L} a_f r^2 - \frac{b_f L + a_f A_L D_{AB}^L}{L^2} r + C_2 \quad (48)$$

$$y = C_3 e^{\frac{-G - 2\pi h \varepsilon D_{AB}^G}{A_V D_{AB}^G} r} - \frac{1}{2G + 4\pi h \varepsilon D_{AB}^G} a_f r^2 - \frac{b_f (G + 2\pi h \varepsilon D_{AB}^G) - a_f A_V D_{AB}^G}{(G + 2\pi h \varepsilon D_{AB}^G)^2} r + C_4 \quad (49)$$

As the system is stable finally, the mass fractions of the outflow and inflow in the reboiler are equal. The reboiler is

Table 3. Simulation Results of Droplet–Droplet Collision (Liquid Flow Rate: 100 L/h, Gas flow rate: 5 m<sup>3</sup>/h)

Rotor Speed	Position	At $r = 0.06$ m			At $r = 0.1$ m			At $r = 0.15$ m		
		Possible outcomes			Possible Outcomes			Possible Outcomes		
600 (r/min)	\	Bouncing								
	$d_L/m$	4.0402E-04								
	$N_L$	2								
	$d_{sat}$	4.0402E-04								
900 (r/min)	$d_{end}$	4.0402E-04								
	\	Reflexive Separation	Coalescence	Stretching separation	Bouncing					
	$d_L$	2.6935E-04	2.6935E-04	2.6935E-04	2.6935E-04					
	$N_L$	1	1	3	2					
1200 (r/min)	$d_{sat}$	3.3935E-04	3.3935E-04	5.5726E-05	2.6935E-04					
	$d_{end}$	/	/	2.6895E-04	2.6935E-04					
	\	Reflexive Separation	Coalescence	Stretching separation	Bouncing					
	$d_L$	2.0201E-04	2.0201E-04	2.0201E-04	2.0201E-04					
	$N_L$	1	1	3	2					
	$d_{sat}$	2.5452E-04	2.5452E-04	6.2814E-05	2.0201E-04					
	$d_{end}$	/	/	2.0099E-04	/					

$d_L = d_{L1} = d_{L2}$

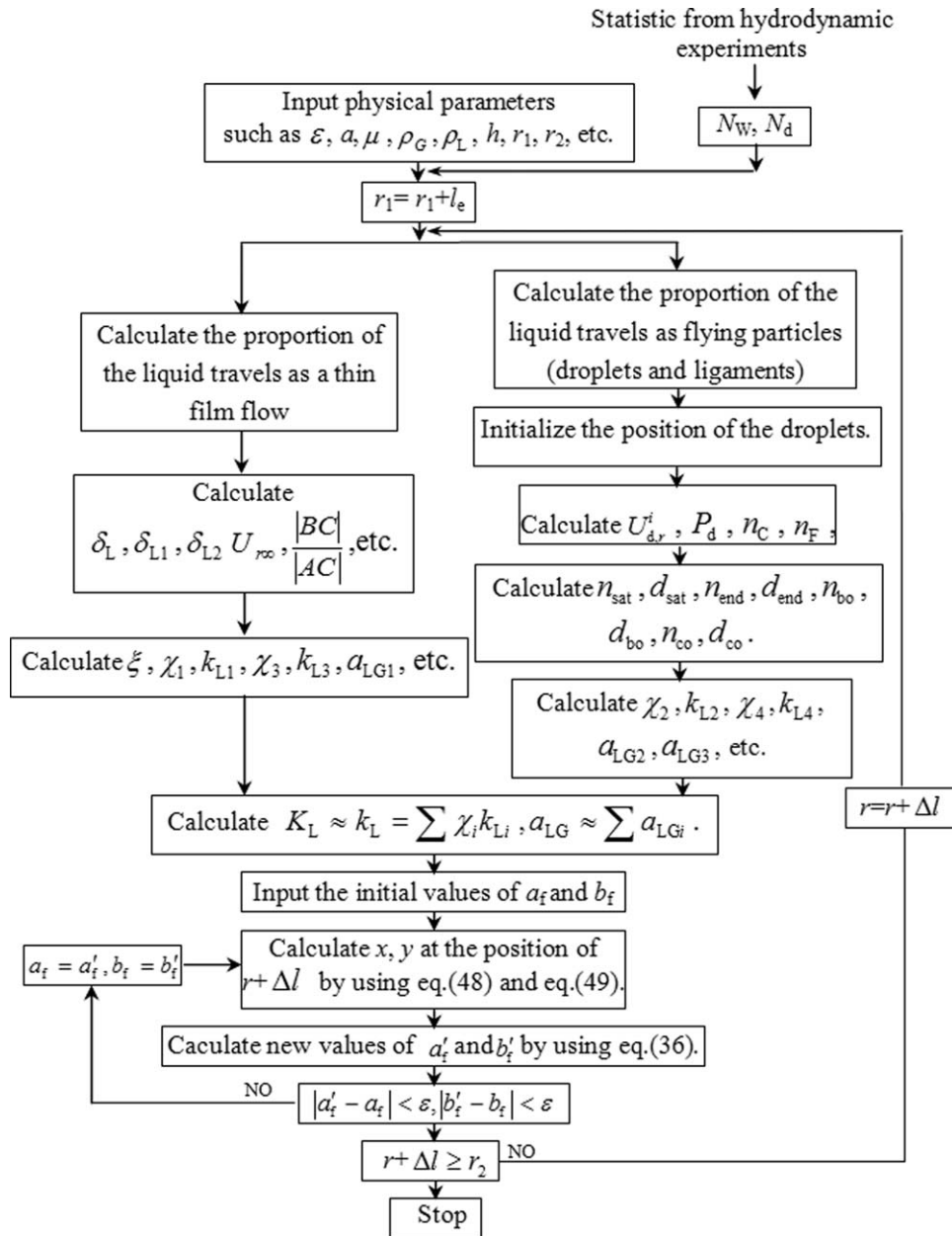


Figure 14. Flow chart for the simulation.

full of the raw material and the liquid holdup of the reboiler is very large. This means that the mass fraction of outflow and inflow in the reboiler almost keeps a constant, that is,  $C_1$ ,  $C_2$ ,  $C_3$ , and  $C_4$  can be obtained by following boundary conditions

$$x|_{r=r_2}=y_{\text{reboiler}}, \quad \left. \frac{\partial x}{\partial r} \right|_{r=r_2}=0 \quad (50)$$

$$y|_{r=r_2}=y_{\text{reboiler}}, \quad \left. \frac{\partial y}{\partial r} \right|_{r=r_2}=0 \quad (51)$$

#### Flow chart for the simulation

Equations 48 and 49 can be used to predict gas and liquid mass fraction in RPB between  $r$  and  $r + \Delta l$ . However,  $a_f$  and  $b_f$  should be calculated in advance. In this article,  $a_f$  and  $b_f$  are given a initial values and checked by Eq. 36 after  $x$  and  $y$  are obtained (trial and error method). To directly describe

the simulation process, the flow chart is shown in Figure 14. In Figure 14, the value of  $\delta_L$ ,  $\delta_{L1}$ ,  $\delta_{L2}$ ,  $U_{\infty}$ ,  $\frac{|BC|}{|AC|}$  and so forth, can be obtained by some hydrodynamic method which have been shown in our previous works in Ref. 16. The value of  $n_{\text{sat}}$ ,  $d_{\text{sat}}$ ,  $n_{\text{end}}$ ,  $d_{\text{end}}$ ,  $n_{\text{bo}}$ ,  $d_{\text{bo}}$ ,  $n_{\text{co}}$ ,  $d_{\text{co}}$  and so forth, can be obtained based on the evaluating parameters  $C_{\text{VS}}$ ,  $T$ ,  $We_{\text{LS}}$ , and  $Re_{\text{LS}}$  ( $C_{\text{VS}}$ ,  $T$  by Ref. 24 and  $We_{\text{LS}}$ ,  $Re_{\text{LS}}$  by Ref. 25).

#### Model Validation

Obviously, hydrodynamic models are the foundation of the mass-transfer models. However, in this article, the mass-transfer models for the distillation process are proposed first. Then, to solve the phase interface  $a_{\text{LG}}$  and mass-transfer coefficients  $K_L$  in the mass-transfer model, hydrodynamic models in a RPB are studied. The hydrodynamic models involve the distribution of the gas-liquid two-phase flow





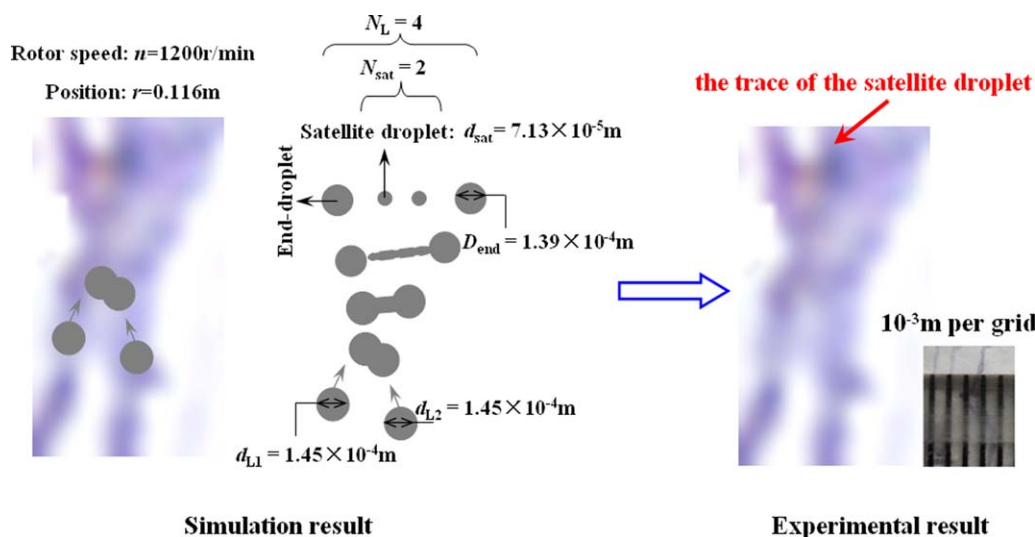


**Figure 17. Comparison of the simulation result with experimental result for separation collision.**

[Color figure can be viewed in the online issue, which is available at [wileyonlinelibrary.com](http://wileyonlinelibrary.com).]

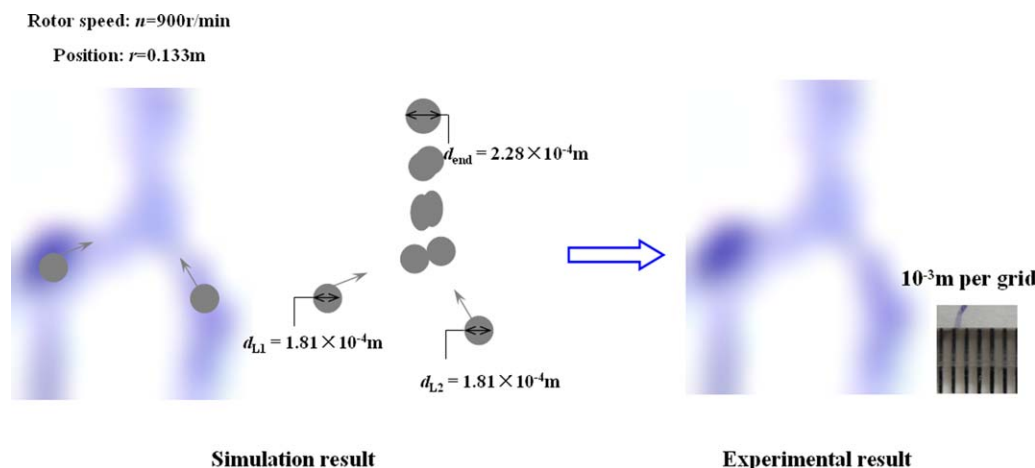
trajectory. It is agreed with the phenomenon of the coalescence collision. Figure 19 shows the comparison of the simulation result with experimental result for the bouncing collision. As shown in Figure 19, two liquid trajectories combine temporarily and separate immediately. It is agreed with the phenomenon of the bouncing collision.

Table 4 presents the value of  $We_{LS}^{0.5} Re_{LS}^{0.25}$  for droplet-packing collision under different operating conditions (gas flow rate, liquid flow rate, and rotor speed) and different positions in RPB. From Table 4, it is found that the value of  $We_{LS}^{0.5} Re_{LS}^{0.25}$  for droplet-packing collision is between 3 and 57. According to the judge criteria listed in previous section, the outcomes of droplet-packing collision are deposition. This means there are not any bouncing and splashing phenomena in RPB when the droplet-packing collision happens. If the droplet splashes and the secondary droplets are produced, there would be a big mark on the paper like the phenomenon of the satellite droplets which are produced by droplet–droplet collision. Similarly, if the bouncing occurs, there would be bouncing mark on the paper. However, it is found that there is not any other mark except one liquid trajectory on the paper (see Figure 3). The only explanation is

that the outcomes of the droplet-packing collisions are deposition.

Table 5 present the value of  $We_{LG}$  for the deformation and breakup of liquid droplets in gas–liquid two-phase flow under different operating conditions (gas flow rate, liquid flow rate, and rotor speed) and different positions in RPB. From Table 5, it is found that the value of  $We_{LG}$  is very small (the magnitude of  $We_{LG}$  is about  $10^{-2}$  m). According to the judge criteria listed in previous section, the outcomes belong to Vibrational mode. As the value of  $We_{LG}$  is so low, it is reasonable to considered that the droplet only deformed and does not have the ability to break up. This conclusion may be supported by the experiment of Wierzba.<sup>58</sup> The droplet behavior of the deformation (flattening) without breakup is shown in Figure 20. The experimental range of Weber Number in Ref. 58 is from 11 to 14. However, the values of  $We_{LG}$  in RPB in this article are much smaller than those values in Ref. 58. As  $We_{LG}$  reflects the ratio of the aerodynamics force by the gas to the interfacial tension of the droplets, it is reasonable to think that the gas has little effect on the liquid state.

In fact, droplet–droplet collision, droplet-packing collision, and droplet breakup should be considered at the same time



**Figure 18. Comparison of the simulation result with experimental result for the coalescence collision.**

[Color figure can be viewed in the online issue, which is available at [wileyonlinelibrary.com](http://wileyonlinelibrary.com).]

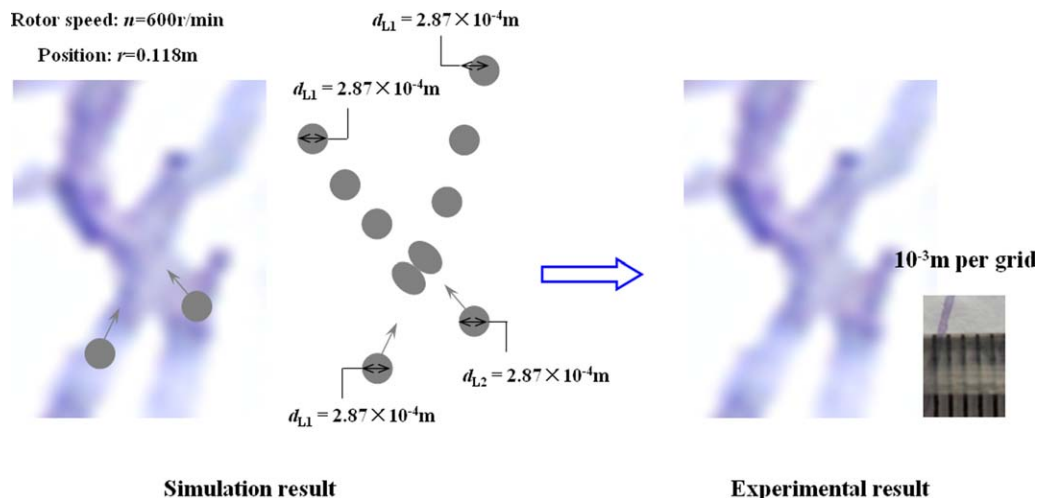


**Figure 19. Comparison of the simulation result with experimental result for the bouncing collision.**

[Color figure can be viewed in the online issue, which is available at [wileyonlinelibrary.com](http://wileyonlinelibrary.com).]

**Table 4. The Value of  $We_{LS}^{0.5} Re_{LS}^{0.25}$  for Droplet–Packing Collisions Under Different Operating Conditions**

	100 (L/h)			200 (L/h)			300 (L/h)		
	At $r = 0.06$ m	At $r = 0.1$ m	At $r = 0.15$ m	At $r = 0.06$ m	At $r = 0.1$ m	At $r = 0.15$ m	At $r = 0.06$ m	At $r = 0.1$ m	At $r = 0.15$ m
5 (m <sup>3</sup> /h)									
600 (r/min)	6.9118	12.7855	15.1217	6.9118	12.7855	15.1217	6.9129	12.7855	15.1217
900 (r/min)	10.3778	19.1873	22.6885	10.3790	19.1873	22.6885	10.3801	19.1873	22.6885
1200 (r/min)	13.8436	25.5885	30.2549	13.8464	25.5885	30.2549	13.8519	25.5886	30.2549
20 (m <sup>3</sup> /h)									
600 (r/min)	6.8933	12.7691	15.1106	6.8933	12.7691	15.1106	6.8944	12.7691	15.1106
900 (r/min)	10.3612	19.1725	22.6786	10.3624	19.1725	22.6786	10.3635	19.1725	22.6786
1200 (r/min)	13.8282	25.5748	30.2458	13.8309	25.5748	30.2458	13.8364	25.5749	30.2458
45 (m <sup>3</sup> /h)									
600 (r/min)	6.8751	12.7522	15.0992	6.8751	12.7522	15.0992	6.8761	12.7522	15.0992
900 (r/min)	10.3445	19.1573	22.6683	10.3457	19.1573	22.6683	10.3468	19.1573	22.6683
1200 (r/min)	13.8126	25.5606	30.2363	13.8153	25.5607	30.2363	13.8208	25.5607	30.2363

when the liquid droplets enter the space among the packings. Above three interacting processes should also be considered (especially the interactive effects among the second generation tiny droplets). However, as the conclusion of droplet–packing collision is deposition and the conclusion of the droplets in the gas stream is deformation, it is reasonable to consider that the tiniest droplets in RPB are probably the satellite droplets which are caused by the

droplet–droplet collision, not by droplet–packing collision or droplet breakup.

Figure 21 shows the simulation results of  $k_{L1}$  and  $k_{L3}$  under a certain operation condition (rotor speed: 900 r/min, liquid flow rate: 40 L/h). As shown in Figure 21, the values of  $k_{L1}$  and  $k_{L3}$  increase with the increase of radii. This is because the centrifugal force increases with the radii, which causes thickness of the liquid film and size of the droplets

**Table 5. The Value of  $We_{LG}$  for the Deformation and Breakup of Liquid Droplets in Gas–Liquid Two-Phase Flow Under Different Operating Conditions**

	100 (L/h)			200 (L/h)			300 (L/h)		
	At $r = 0.06$ m	At $r = 0.1$ m	At $r = 0.15$ m	At $r = 0.06$ m	At $r = 0.1$ m	At $r = 0.15$ m	At $r = 0.06$ m	At $r = 0.1$ m	At $r = 0.15$ m
5 (m <sup>3</sup> /h)									
600 (r/min)	0.01143	0.01822	0.02062	0.01143	0.01822	0.02062	0.01143	0.01822	0.02062
900 (r/min)	0.01584	0.02646	0.03038	0.01584	0.02646	0.03038	0.01584	0.02646	0.03038
1200 (r/min)	0.02028	0.03471	0.04014	0.02029	0.03471	0.04014	0.02029	0.03471	0.04014
20 (m <sup>3</sup> /h)									
600 (r/min)	0.02079	0.02389	0.02415	0.02079	0.02389	0.02415	0.02079	0.02389	0.02415
900 (r/min)	0.02441	0.03192	0.03382	0.02441	0.03192	0.03382	0.02442	0.03192	0.03382
1200 (r/min)	0.02846	0.04006	0.04354	0.02847	0.04006	0.04354	0.02847	0.04006	0.04354
45 (m <sup>3</sup> /h)									
600 (r/min)	0.04262	0.03507	0.03064	0.04262	0.03507	0.03064	0.04262	0.03507	0.03064
900 (r/min)	0.04283	0.04216	0.03999	0.04283	0.04216	0.03999	0.04283	0.04216	0.03999
1200 (r/min)	0.04518	0.04984	0.04954	0.04519	0.04984	0.04954	0.04520	0.04984	0.04954

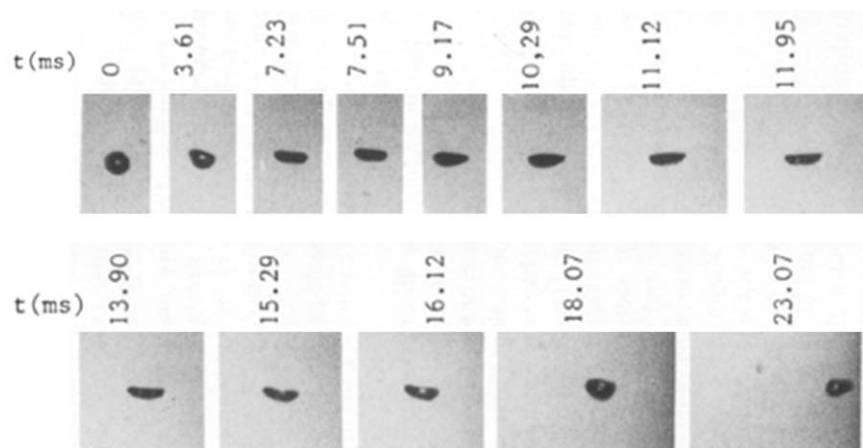


Figure 20. The phenomenon of the droplet behavior of the deformation (flattening) without breakup (by Wierzb<sup>58</sup>).

decrease markedly. According to the simulation in Figure 21, the magnitude of  $k_{L1}$  is about  $10^{-2}$ – $10^{-1}$  cm/s, whereas the magnitude of  $k_{L3}$  is about  $10^{-1}$ – $10^0$  cm/s. That is,  $k_{L3} \gg k_{L1}$ . Therefore, it is unreasonable to consider the whole liquid film flow as laminar flow.

As shown in Figure 22, the flying droplets in the space among the packings are divided into three stages: the first stage is the droplet forming stage, the third stage is that the droplet is approaching the solid surface, and the second stage is the process within the two stages above. In the first stage, the mass-transfer coefficient is rather high. This is because there are strong oscillation and distortion in the droplets when the droplets are just thrown away from packings, which cause the higher mass-transfer coefficient during the initial stages of the droplets formation. The mass-transfer coefficient is decreased sharply with the time at the first stage, and then remain a low value when it enters the second

stage. In the second stage, droplet–droplet collisions may occur. If the droplet–droplet collisions occur, the new satellite droplets may be produced (or some other momentum and mass exchanges may occur between droplets), which may also cause the high mass-transfer coefficient. The process of the droplet approaching the solid surface is called the third stage. This process can be deemed as the reverse process of droplets forming. Therefore, the values of mass-transfer coefficient are distributed symmetrically in first and third stages, which are shown in Figure 22. The magnitude of  $K_L$  by simulation in this article is  $10^{-2}$ – $10^0$  cm/s, which agrees with those reported by Chen and Tong<sup>59</sup> and Munjal et al.<sup>60</sup> (in researches of Chen and Tong,  $K_L$  is about 0.086–0.11 cm/s. In researches of Munjal et al.,  $K_L$  is about 0.08–0.1 cm/s).

Figures 23 and 24 show the comparison of the simulation results with the experimental results of distillation under different rotor speeds and different liquid flow rates, respectively. As shown in Figures 23 and 24, the ethanol

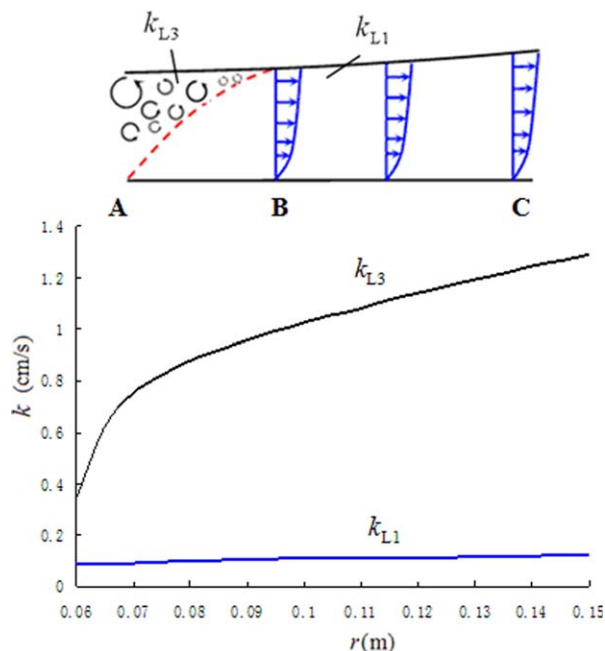


Figure 21. Simulation results of  $k_{L1}$  and  $k_{L3}$  under a certain operational condition.

[Color figure can be viewed in the online issue, which is available at [wileyonlinelibrary.com](http://wileyonlinelibrary.com).]

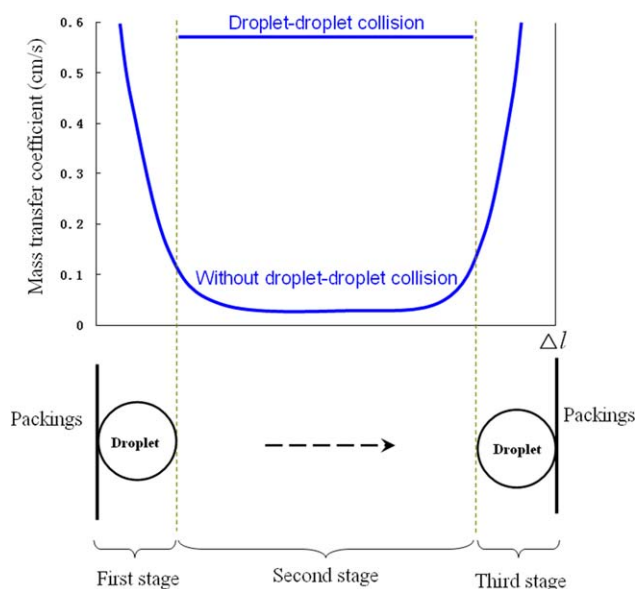
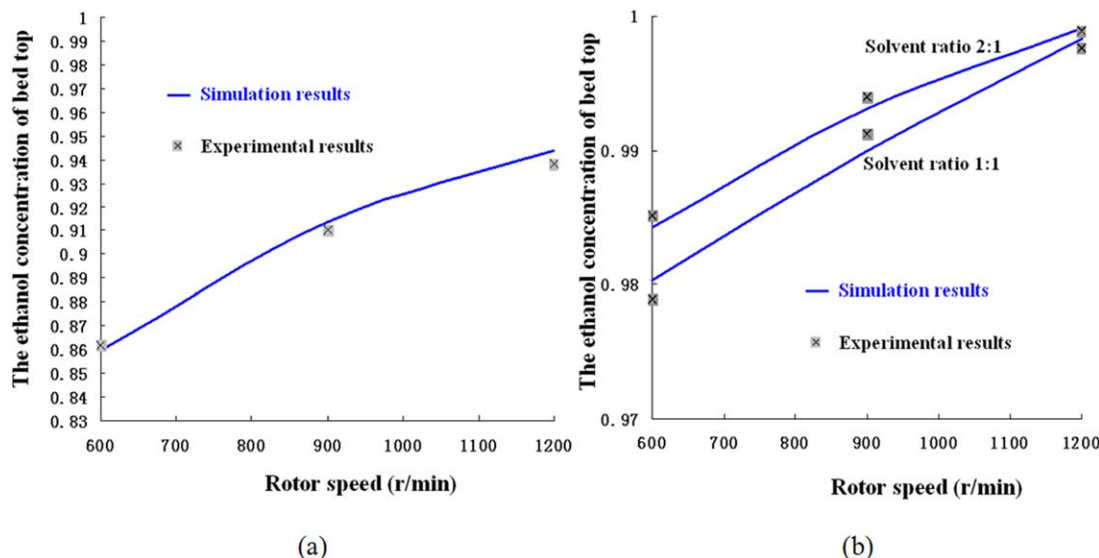


Figure 22. The flying droplets in the space among the packing are divided into three stages.

[Color figure can be viewed in the online issue, which is available at [wileyonlinelibrary.com](http://wileyonlinelibrary.com).]



**Figure 23.** The comparison of the simulation result with experimental result under different rotor speeds: (a) distillation; (b) extractive distillation.

[Color figure can be viewed in the online issue, which is available at [wileyonlinelibrary.com](http://wileyonlinelibrary.com).]

concentrations at bed top are less than 95% without extracting agent because water–ethanol is an azeotropic mixture. Using ethylene glycol as an extracting agent, the azeotropic point of ethanol–water system disappears and the higher concentrations of ethanol are obtained. Both Figures 23 and 24 show that the results of simulation agree well with the experimental results, which prove that both hydrodynamic model and mass-transfer model can better describe the gas–liquid two-phase flow and mass-transfer process in RPB.

As shown in Figure 23, the ethanol concentration at bed top is increasing with the rotor speed. This phenomenon may be explained by the changing rule of the mass-transfer coefficient  $K_L$ . The reason is that, as the rotor speed increases, the velocity of the liquid in RPB is increased, resulting that the size of droplet is getting smaller and the thickness of the liquid film is also getting thinner. These results make  $K_L$  increasing.

However, as shown in Figure 24, the ethanol concentration at bed top is nearly unchanged with the liquid flow rate. To illustrate the point, Figures 23 and 24 are melded into Figure 25. As shown in Figure 25, the effect of rotor speed on the mass-transfer coefficient is greater than that of liquid flow rate obviously. This is because the liquid velocity in RPB almost has nothing to do with the liquid flow rate (see Ref. 16). On the one hand, the thickness liquid film is increasing when the liquid flow rate is increasing, which may make  $K_L$  decrease. On the other hand, the number of droplets and the number of liquid trajectories increase when the liquid flow rate is increased, this makes the frequency of droplet–droplet collisions increases. Above two factors counterbalance with

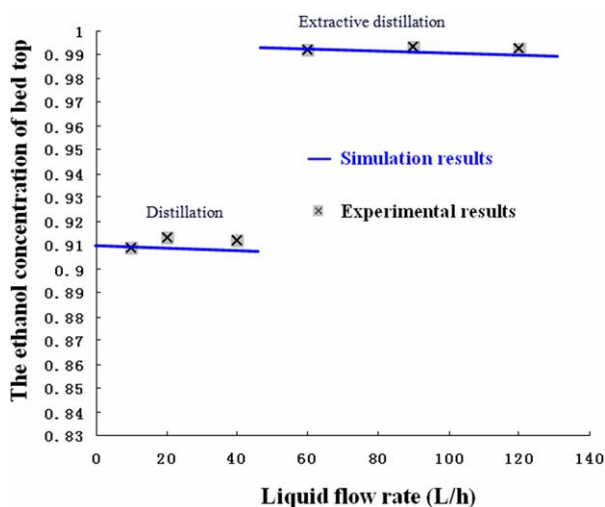


**Figure 24.** Comparison of the simulation result with experimental result under different liquid flow rates.

[Color figure can be viewed in the online issue, which is available at [wileyonlinelibrary.com](http://wileyonlinelibrary.com).]

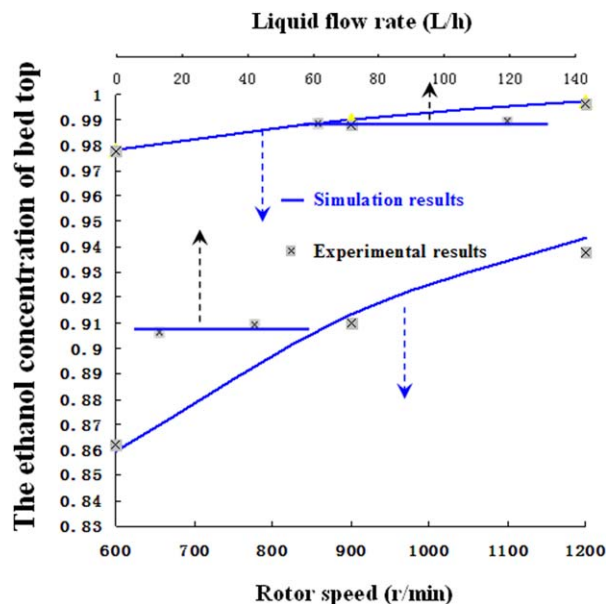


**Figure 25.** Comparison of rotor speed effect with liquid flow rate effect on the ethanol concentration of bed top.

[Color figure can be viewed in the online issue, which is available at [wileyonlinelibrary.com](http://wileyonlinelibrary.com).]



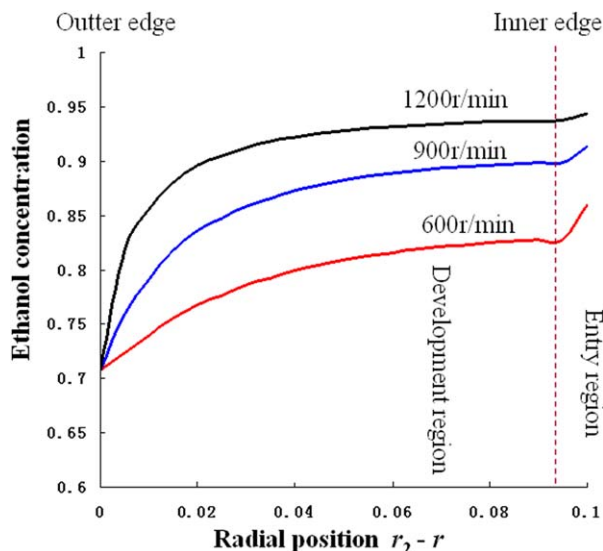


**Figure 26. The concentration distribution of ethanol along the rotor radial under different rotor speeds.**

[Color figure can be viewed in the online issue, which is available at [wileyonlinelibrary.com](http://wileyonlinelibrary.com).]

each other and make  $K_L$  nearly unchanged with the liquid flow rate.

Figure 26 shows the concentration distribution of ethanol along the rotor radial under different rotor speeds. As shown in Figure 26, the ethanol concentration decreases with the radii and the ethanol concentration reaches a maximum in the inner edge of the rotor ( $r = r_1$ ). The curve lines can be divided into two regions (entry region and development region). By simulation, it is found that the curve line of ethanol concentrations increase sharply in the entry region. This indicates that the mass-transfer efficiency in the entry region is very high. This conclusion may be supported by the conclusion of Zhu et al.<sup>61</sup> and Zhang et al.<sup>11</sup> The reason may be explained by the large gas–liquid interface surface in the entry region. As shown in Figure 27, the packings are almost wetted by the liquid totally due to the great relative movement (the magnitude of the relative velocity in this article is about 1–10 m/s) between the liquid and the packings along the circumferential direction in entry region. As two-phase flow fluid interface  $a_{LG}$  is very large in entry region, the

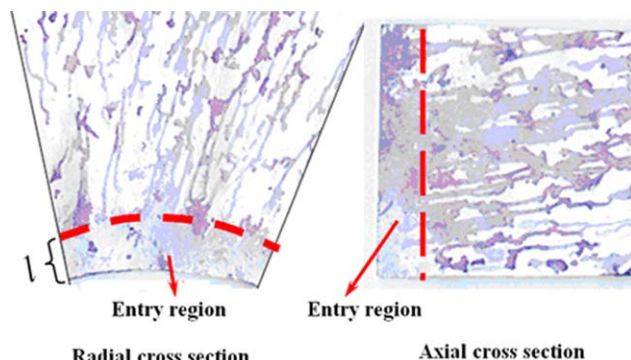


**Figure 27. The large gas–liquid interface surface in entry region.**

[Color figure can be viewed in the online issue, which is available at [wileyonlinelibrary.com](http://wileyonlinelibrary.com).]

impetus of mass transfer is also getting larger, which makes the ethanol concentration increase sharply in entry region.

## Conclusions

The frequency of droplet–droplet collisions per unit radial length and per unit liquid trajectory and its change rules are obtained by the experimental and statistical method. By experiment and simulation, the type of the collision outcomes, the size of the satellite droplets, the number of the satellite droplets, the size of the two end droplets, and some other complex hydrodynamic characteristics for the droplets in RPB are also obtained. The values of  $We_{LS}^{0.5} Re_{LS}^{0.25}$  for droplet–packing collisions in RPB are between 3 and 57 which are obtained by simulation. By theoretical analysis and experiment, the conclusion is that the frequency of droplet–packing collisions is very high and the outcomes of droplet–packing collisions are deposition. The gas has little effect on the liquid state and the liquid droplets only deformed when it fly through the space among the packing in RPB. The tiniest droplets in RPB are probably the satellite droplets which are caused by the droplet–droplet collision, not by the aerodynamics force by the gas or droplet–packing collisions. The collisions improve the mass transfer effectively and the satellite droplets can increase the two-phase flow fluid interface greatly.

The liquid film flow on the packings surface can be divided into two distinctly different segments according to the boundary layer development (segment AB and BC). The mass-transfer coefficient in segment AB is much higher than that in segment BC. The flying droplets in the space among the packings are divided into three stages. The first stage is the droplet forming stage whose mass-transfer coefficient is higher. The mass-transfer coefficient is much lower after the droplet has formed, which is called the second stage. The third stage is that the droplet is approaching the solid surface, whose mass-transfer coefficient also is higher. Droplet–droplet collisions in RPB can greatly enhance the mass-transfer coefficient. After collisions, the satellite droplets may be produced, which not only improve the mass-transfer coefficient greatly, but also increase the gas–liquid mass-transfer interface greatly.

Based on the hydrodynamic results, mathematical models for the mass transfer in RPB are proposed in this work. Mass-transfer experiments in RPB are also carried out using ethanol–water solution under different operating conditions. By comparison, the results of simulation agree well with the results of the experiment, and show that both hydrodynamic model and mass-transfer model can better describe the gas–liquid two-phase flow and mass-transfer process. In fact, the effect of the thermal energy transport in RPB is also critical to determine the mass transfer when RPB is applied to distillation, however, it has not been considered in this article for the limitation of thesis. Therefore, one of the remained missions is to consider heat transfer in RPB for using the devise to distillation.

## Acknowledgment

This work was supported by the fund projects of Fujian Province Education Office (serial number: 2012-XY-8).

## Notation

$a$  = specific surface area of the packing,  $m^2/m^3$   
 $a_d$  = surface area of the liquid droplet,  $m^2$   
 $a_f$  = constant

$a_{LG}$  = two-phase flow fluid interface,  $m^2$   
 $A_L$  = passing section of the liquid flow,  $m^2$   
 $A_V$  = passing section of the gas flow,  $m^2$   
 $b_f$  = constant  
 $c_1, c_2, \dots, c_n$  = constants  
 $c_A$  = mass concentration of the component A  
 $c_{A,0}$  = initial concentration inside the drop of the component A  
 $c_{A,\infty}$  = mass concentration of the component A outside the boundary layer  
 $c_{As}$  = mass concentration of the component A on the solid surface  
 $C_1, C_2, \dots, C_n$  = constants  
 $C_{VS}$  = separation volume coefficient  
 $d_{bo}$  = diameter of the bouncing droplets, m  
 $d_{co}$  = diameter of the coalescence droplets, m  
 $d_e$  = hydraulic diameter, m  
 $d_{end}$  = diameter of the end droplet, m  
 $d_{L1}$  = diameter of the larger droplet, m  
 $d_{L2}$  = diameter of the smaller droplet, m  
 $d_L^i$  = initial diameter of the ligament, m  
 $d_L^r$  = ligament diameter at the breakup, m  
 $d_m$  = droplet diameter, m  
 $d_{sat}$  = diameter of the satellite droplets formed from the ligament breakup, m  
 $D_{AB}^G$  = gas diffusion coefficient,  $m^2/s$   
 $D_{AB}^L$  = liquid diffusion coefficient,  $m^2/s$   
 $E$  = strain rate tensor  
 $E_d'$  = dissipated energy after droplet-packing collision  
 $E_k$  = kinetic energy before droplet-packing collision  
 $E_k'$  = kinetic energy after droplet-packing collision  
 $E_p$  = potential energy before droplet-packing collision  
 $E_p'$  = potential energy after droplet-packing collision  
 $E_s$  = surface energy before droplet-packing collision  
 $E_s'$  = surface energy after droplet-packing collision  
 $E_{dissip}$  = viscous dissipation  
 $E_{stretch}$  = total effective stretching kinetic energy  
 $E_{surten}$  = surface energy in the region of interaction  
 $FO$  = Fourier number for the mass transfer  
 $h$  = height of the bed, m  
 $H_0$  = liquid holdup per unit volume  
 $H_0$  = gas holdup per unit volume  
 $k_G$  = mass-transfer coefficient in gas phase,  $cm/s$   
 $k_L$  = mass-transfer coefficient in liquid phase,  $cm/s$   
 $k_{L1}$  = mass-transfer coefficient of the liquid boundary layer,  $cm/s$   
 $k_{L2}$  = mass-transfer coefficient of the drop formation,  $cm/s$   
 $k_{L3}$  = mass-transfer coefficient of the droplet approaching the solid surface,  $cm/s$   
 $k_{L4}$  = mass-transfer coefficient for the droplet flying through the space among the packings,  $cm/s$   
 $k_s$  = fit parameter  
 $K_L$  = overall mass-transfer coefficient,  $cm/s$   
 $l$  = length of the entry region along the radial direction, m  
 $l_1$  = flying distance of the liquid ligament in the space among the packing after collision, m  
 $L$  = flow rate of mixed solution,  $m^3/s$   
 $L_e$  = width of the liquid trajectory, m  
 $\Delta l$  = moving distance of the liquid during  $\Delta t$  along the radial direction m  
 $\Delta l_d$  = small radial length near the outer edge of the flabellate paper, m  
 $m$  = constant  
 $M_A$  = total transferred mass  
 $n_{bo}$  = number of the bouncing droplets during  $r-r + \Delta l$   
 $n_{co}$  = number of the coalescence droplets during  $r-r + \Delta l$   
 $n_C$  = number of the droplets that collision during  $r-r + \Delta l$   
 $n_F$  = number of the flying droplets before droplet-droplet collision  
 $n_{sat}$  = number of all satellite droplets during  $r-r + \Delta l$   
 $n_{end}$  = number of all end droplets during  $r-r + \Delta l$   
 $n_w$  = number of the liquid trajectories  
 $N_d$  = whole number of the intersection for the liquid trajectories in statistic region  
 $N_{sat}$  = number of satellite droplets  
 $N_w$  = whole number of liquid trajectories in statistic region  
 $Oh_{LS}$  = Ohnesorge number in droplet-packing collision

$P_d$  = collision frequency per unit radial length and per unit liquid trajectory  
 $r$  = radius, m  
 $r_A$  = rate of the formation of the component A in the chemical reactions  
 $Re_{LS}$  = Reynolds number in droplet-packing collision  
 $t$  = time, s  
 $t_{d,r}$  = time of the breakup of the ligament, s  
 $t_f$  = drop formation time  
 $t_{tr}$  = travel time of the liquid droplet among the space of packings, s  
 $T$  = time scale  
 $U$  = velocity of the liquid in the irrigated bed,  $m/s$   
 $U_{d,r}^i$  = velocity of the liquid droplets at the radial position of  $r$ ,  $m/s$   
 $U_{d,r,n}^i$  = the normal components of the velocity for the droplets at the radial position of  $r$ ,  $m/s$   
 $U_{d,r}^i$  = velocity of the liquid ligament after collision at the radial position of  $r$ ,  $m/s$   
 $U_{r\infty}$  = velocity of the undisturbed liquid flow at the radial position of  $r$ ,  $m/s$   
 $|\bar{U}_{12}|$  = relative velocity between the two droplets,  $m/s$   
 $\nu$  = kinematic viscosity,  $m^2/s$   
 $V$  = velocity of the gas in the unirrigated bed,  $m/s$   
 $V_G$  = gas flow rate,  $m^3/s$   
 $V_{r,z,\theta}$  = velocity of the gas whose coordinate position is  $(r, z, \theta)$  in RPB,  $m/s$   
 $V_{r,max}$  = maximal velocity of the gas at the radial position of  $r$ ,  $m/s$   
 $We_{LL}$  = Weber number between two droplets  
 $We_{LS}$  = Weber number in droplet-packing collision  
 $We_{LS,r,z,\theta}$  = Weber number at any position  $(r, z, \theta)$  in RPB in the droplet deformation process

## Greek letters

$\beta$  = chance for the liquid enters the space among the packing  
 $\delta_D$  = thickness of the concentration boundary layer, m  
 $\delta_L$  = whole thickness of liquid film flow, m  
 $\delta_{L1}$  = thickness of the velocity boundary layer, m  
 $\delta_{L2}$  = thickness of the undisturbed liquid flow, m  
 $\varepsilon$  = porosity  
 $\mu$  = fluid viscosity,  $kg/m \cdot s$   
 $\zeta$  = ratio of concentration boundary layer to velocity boundary layer  
 $\rho_G$  = gas density,  $kg/m^3$   
 $\rho_L$  = liquid density,  $kg/m^3$   
 $\chi_1$  = proportion of the laminar flow in the whole liquid flow  
 $\chi_2$  = proportion of the drop formation in the whole liquid flow  
 $\chi_3$  = proportion of the droplet approaching the solid surface in the whole liquid flow  
 $\psi_l$  = volume lost from the smaller and the larger droplets to form the ligament  
 $\omega$  = rotational speed,  $rad/s$

## Literature Cited

- Ramshaw C, Mallinson RH. Mass transfer process. U.S. Patent 4,283,255, 1981.
- Munjal S, Dudukovic MP, Ramachandran P. Mass-transfer in rotating packed beds. I. Development of gas-liquid and liquid-solid mass-transfer correlations. *Chem Eng Sci.* 1989;44:2245–2256.
- Chen JF, Gao H, Zou HK, Chu GW, Zhang L, Shao L, Xiang Y, Wu YX. Cationic polymerization in rotating packed bed reactor: experimental and modeling. *AIChE J.* 2010;56:1053–1062.
- Lin CC, Liu WT, Tan CS. Removal of carbon dioxide by absorption in a rotating packed bed. *Ind Eng Chem Res.* 2003;42:2381–2386.
- Chen JF, Shao L, Guo F, Wang XM. Synthesis of nano-fibers of aluminum hydroxide in novel rotating packed bed reactor. *Chem Eng Sci.* 2003;58:569–575.
- Dipendu S. Prediction of mass transfer coefficient in rotating bed contactor (Higee) using artificial neural network. *Heat Mass Transfer.* 2009;45:451–457.
- Kelleher T, Fair JR. Distillation studies in a high-gravity contactor. *Ind Eng Chem Res.* 1996;35:4646–4655.
- Lin CC, Ho TJ, Liu WT. Distillation in a rotating packed bed. *J Chem Eng Jpn.* 2002;35:1298–1304.

9. Burns JR, Ramshaw C. Process intensification: visual study of liquid maldistribution in rotating packed beds. *Chem Eng Sci.* 1996;51:1347–1352.
10. Zhang J. *Experiment and Modelling of Liquid Flow and Mass Transfer in Rotating Packed Bed*. Ph. D. Dissertation. Beijing: Beijing University of Chemical Technology, 1996.
11. Zhang J, Guo K, Guo F, Zhu JS, Zheng C. Experimental study about flow of liquid in rotating packed bed. *J Chem Eng Chin Univ.* 2000;14:378–381.
12. Mochida T, Kukida Y, Imamura K. Spray drying. Translated by Zhang Youguo. Suzhou: Jiangsu Publishing Company of Science and Technology, 1982.
13. Friedman SJ, Gluckert FA, Marshall WR. Centrifugal disk atomization. *Chem Eng Prog.* 1952;48:181.
14. Chen HH, Zeng YY. *Applying Study of Rotating Packed Bed*. Changsha: National University of Defence Technology Press, 2002.
15. Yan ZY, Lin C, Ruan Q. Hydrodynamics in a rotating packed bed. I. A novel experimental method. *Ind Eng Chem Res.* 2012;51:10472–10481.
16. Yan ZY, Ruan Q, Lin C. Hydrodynamics in a rotating packed bed. II. A mathematical model. *Ind Eng Chem Res.* 2012;51:10482–10491.
17. Sommerfeld M. Validation of a stochastic Lagrangian modelling approach for inter-particle collisions in homogeneous isotropic turbulence. *Int J Multiphase Flow.* 2001;27:1829–1858.
18. O'Rourke PJ. Collective drop effects on vaporizing liquid sprays, Ph. D. Dissertation. New Mexico (USA): Princeton University, 1981.
19. Kim S, Lee DJ, Lee CS. Modeling of binary droplet collisions for application to inter-impingement sprays. *Int J Multiphase Flow.* 2009;35:533–549.
20. Ashgriz N, Poo JY. Coalescence and separation in binary collisions of liquid drops. *J Fluid Mech.* 1990;221:183–204.
21. Brazier-Smith PR, Jennings SG, Latham J. The interaction of falling rain drops: coalescence. *Proc R Soc London.* 1972;A326:393–408.
22. Qian J, Law CK. Regimes of coalescence and separation in droplet collision. *J Fluid Mech.* 1997;331:59–80.
23. Tennison PJ, Georjon TL, Farrell PV, Reitz RD. An experimental and numerical study of sprays from a common rail injection system for use in an HSDI diesel engine. *SAE Transactions.* 1998;106:1228–1244.
24. Munnannur A, Reitz RD. A new predictive model for fragmenting and nonfragmenting binary droplet collisions. *Int J Multiphase Flow.* 2007;33:873–896.
25. Escure C, Vardelle M, Fauchais P. Experimental and theoretical study of the impact of alumina droplets on cold and hot substrates. *Plasma Chem Plasma Process.* 2003;23:185–221.
26. Zhang X, Osman A. Dynamic surface tension effects in impact of a drop with a solid surface. *J Colloid Interface Sci.* 1997;187:166–178.
27. Mundo C, Sommerfeld M, Tropea C. Droplet-wall collisions: experimental studies of the deformation and breakup process. *Int J Multiphase Flow.* 1995;21:151–173.
28. Chandra S, Avedisian CT. On the collision of a droplet with a solid surface. *Proc R Soc London.* 1991;A432:13–41.
29. Mundo C, Sommerfeld M, Tropea C. Experimental studies of deposition and splashing of small liquid droplets impinging on a flat surface. *Proceedings of the 6th International Conference on Liquid Atomization and Spray Systems*. Rouen: ILASS (Institute for Liquid Atomization and Spray Systems), 1994.
30. Lavergne G, Platet B. Study of the impact of droplets on a heated wall (in French). Final Report. Nbl/2401/CERT/DERMES, 1991.
31. Pilch M, Erdman CA. Use of breakup time data and velocity history data to predict the maximum size of stable fragments for acceleration-induced breakup of a liquid drop. *Int J Multiphase Flow.* 1987;13:741–757.
32. Hsiang LP, Faeth GM. Near-limit drop deformation and secondary breakup. *Int J Multiphase Flow.* 1992;18:635–652.
33. Hsiang LP, Faeth GM. Drop properties after secondary breakup. *Int J Multiphase Flow.* 1993;19:721–735.
34. Hsiang LP, Faeth GM. Drop deformation and breakup due to shock wave and steady disturbances. *Int J Multiphase Flow.* 1995;21:545–560.
35. Theofanous TG, Li GJ, Dinh TN. Aerobreakup in rarefied supersonic gas flows. *J Fluid Eng T ASME.* 2004;126:516–527.
36. Zheng C, Guo K, Feng Y, Yang C, Gardener NC. Pressure drop of centripetal gas flow through rotating beds. *Ind Eng Chem Res.* 2000;39:829–834.
37. Sandilya P, Rao DP, Sharma A. Gas-phase mass transfer in a centrifugal contactor. *Ind Eng Chem Res.* 2001;40:384–392.
38. Liu HS, Lin CC, Wu SC, Hsu HW. Characteristics of a rotating packed bed. *Ind Eng Chem Res.* 1996;35:3590–3596.
39. Rao DP, Bhowal A, Goswami PS. Process intensification in rotating packed beds (HIGEE): an appraisal. *Ind Eng Chem Res.* 2004;43:1150.
40. Rajan SM, Heideger WJ. Drop formation mass transfer. *AIChE J.* 2004;17:202–206.
41. Heertjes PM, deNie LH. The mechanism of mass transfer during formation, release and coalescence of drops. Part I—mass transfer to drops formed at a moderate speed. *Chem Eng Sci.* 1966;21:755–768.
42. Heertjes PM, Holve WA, Talsma H. Mass transfer between isobutanol and water in a spray-column. *Chem Eng Sci.* 1954;3:122–142.
43. Popovich AT, Jervis RE, Trass O. Mass transfer during single drop formation. *Chem Eng Sci.* 1964;19:357–365.
44. Licht W, Conway JB. Mechanism of solute transfer in spray towers. *Ind Eng Chem.* 1950;42:1151–1157.
45. Licht W, Pansing WF. Solute transfer from single drops in liquid-liquid extraction. *Ind Eng Chem.* 1953;45:1885–1896.
46. Javadi A, Bastani D, Taeibi-Rahni M. Mass transfer during drop formation on the nozzle: new flow expansion model. *AIChE J.* 2006;52:895–910.
47. Walia DS, Vir D. Extraction from single forming drops. *Chem Eng J.* 1976;12:133–141.
48. Walia DS, Vir D. Interphase mass transfer during drop or bubble formation. *Chem Eng Sci.* 1976;31:525–533.
49. Higbie R. The rate of absorption of a pure gas into a still liquid during short periods of exposure. *Trans Am Inst Chem Eng.* 1935;31:365–377.
50. Sherwood TK, Pigford RL, Wilke CR. Mass Transfer. New York: McGraw-Hill, 1975.
51. Chermisinoff NP. Handbook of heat and mass transfer. Vol. II. Mass Transfer and Reactor Design. Houston: Gulf Publishing Company, 1986.
52. Xie SS, Gu HP, Xiao RZ. Transport Processes in Chemical Engineering. Beijing: Chemical Industry Press, 2007.
53. Guo F. Characteristics of hydrodynamics and mass transfer in cross flow rotating packed bed. Ph. D. Dissertation. Beijing: Beijing University of Chemical Technology, 1996.
54. Kang RC, Liu YZ, Liu ZH, Li P, Diao JX. Study on the process of gas-film controlled mass transfer in sealed cross-flow rotating packed bed. *Chem Eng.* 2007;35:1–5.
55. Basic A, Dudukovic MP. Liquid holdup in rotating packed beds: examination of the film flow assumption. *AIChE J.* 1995;41:301–316.
56. Burns JR, Jamil JN, Ramshaw C. Process intensification: operating characteristics of rotating packed beds determination of liquid hold-up for a high-voidage structured packing. *Chem Eng Sci.* 2000;55:2401–2415.
57. Zhou LH, Liu YZ, Li GM. A new method of determining liquid hold-up in rotating packed bed. *Mod Chem Ind.* 2010;30:91–94.
58. Wierzbna A. Deformation and breakup of liquid drops in a gas stream at nearly critical Weber numbers. *Exp Fluids.* 1990;9:59–64.
59. Chen ZQ, Tong ZQ. Helical rotating absorber (II). Mass transfer coefficients of flue gas desulphurization. *J Chem Ind Eng.* 1996;47:758–762.
60. Munjal S, Dudukovic MP, Ramachandran P. Mass-transfer in rotating packed beds. II. Experimental results and comparison with theory and gravity flow. *Chem Eng Sci.* 1989;44:2257–2268.
61. Zhu JS, Guo K, Fen YD, Zheng C. Modeling of mass transfer in rotating packed bed. *J Chem Eng Chin Univ.* 1998;12:219–225.

Manuscript received Sept. 5, 2013, and revision received Feb. 24, 2014.